A Model for the Influence of Wind and Oceanic Currents on the Size of a Steady-State Latent Heat Coastal Polynya

A. J. WILLMOTT AND M. A. MORALES MAQUEDA

Department of Mathematics, Keele University, Keele, United Kingdom

M. S. DARBY

Department of Mathematics, University of Exeter, North Park Road, Exeter, United Kingdom

(Manuscript received 2 September 1996, in final form 14 April 1997)

ABSTRACT

This paper presents a model for determining the size and shape of a steady-state latent heat coastal polynya in terms of the following free parameters: 1) the frazil ice production rate (F); 2) the wind stress ($\boldsymbol{\tau}$); 3) the surface ocean velocity field ($\mathbf{u}$); 4) the offshore consolidated thin ice transport ($\mathbf{T}$); 5) the coastline shape; and 6) the intersection of the polynya ice edge with the coastline, all of which must be prescribed. Frazil ice trajectories are determined via the free-drift ice momentum balance. Analytical solutions for the polynya shape are derived for a straight coastline in the special case when $\mathbf{u}$, $\mathbf{T}$, and $\boldsymbol{\tau}$ are uniform in the alongshore direction and the rotation of the earth is neglected. When the latter constraint is relaxed, an expression for the asymptotic uniform polynya width is obtained. An expression for the alongshore adjustment length scale of the polynya associated with alongshore variations in the coastline shape, $\mathbf{u}$, $\mathbf{T}$, and $\boldsymbol{\tau}$ is derived, with rotation of the earth included. By considering a wedge-shaped ocean domain in which the ocean velocity is nondivergent and irrotational it is demonstrated that (i) a polynya solution does not always exist and (ii) a point (S, say) can exist where the frazil ice and thin ice transports are equal. When S exists, all possible polynya ice edge curves will pass through this point. The model is applied to simulate the wind-driven polynya that sometimes forms off the northern Greenland coast during winter and early spring between the Henrik Krøyer Islands and the Ob Bank. Because of fundamental couplings between the free parameters listed above, one should be cautious in drawing inferences on the physical behavior of the polynya. However, the model is useful in revealing the sensitivity of the polynya to variations in the prescribed forcing fields.

1. Introduction

A latent heat coastal polynya is a region of nearly ice-free water located between the coast (or land fast ice) and the sea ice pack. The polynya is the result of the offshore advection of ice by winds and/or oceanic currents. The size of the polynya is governed by the balance between the export of new ice away from the coast and the production of frazil ice inside the polynya. Ice is created over the entire area of the polynya, and it is often observed to be organized in streamers along convergence lines associated with Langmuir circulation (Martin and Kauffman 1981). Coastal polynyas play an important role in controlling the local heat exchange between the atmosphere and the ocean, they largely contribute to the formation of intermediate and deep waters (through brine rejection when sea ice forms), and they are sites of high biological activity (Smith et al. 1990).

From the simple, but nevertheless perceptive, models of Lebedev (1968) and Pease (1987) for the maintenance of a latent heat coastal polynya, a number of process models have been developed that study the influence of oceanic sensible heat (Mysak and Huang 1992; Darby et al. 1994, hereafter referred to as DWM), coastline orientation (DWM; Darby et al. 1995, hereafter referred to as DWS), and the direction of drift of frazil ice (DWM and DWS) on a polynya. The purpose of this paper is to present a theory for the maintenance of a steady-state latent heat coastal polynya that explicitly incorporates the effects of winds and upper-ocean circulation on the frazil ice motion.

Steady-state models for the maintenance of a latent heat coastal polynya are useful because the Pease (1987) adjustment timescale over which a steady state is reached is of the order of 1 to 2 days, which is short compared with the timescale of low-period atmospheric storms (Ou 1988). Latent heat coastal polynyas are found, for instance, in the northern Bering Sea, along the East Greenland coast, over the Siberian shelf, and in a large number of sites around Antarctica (e.g., Smith et al. 1990; Gordon and Comiso 1988). In some coastal

Corresponding author address: Dr. A. J. Willmott, Department of Mathematics, Keele University, Keele, Staffordshire L69 3BX, United Kingdom.
E-mail: a.j.willmott@keele.ac.uk

polynyas, vertical mixing or upwelling of deeper warm water produce an oceanic sensible heat flux, which can play a role in the maintenance of the polynya. Allowing for the effects of sensible heat associated with coastal upwelling introduces an upwelling timescale (Mysak and Huang 1992), of typically one to two weeks. Therefore, the utility of steady-state models for a combined latent and sensible heat polynya is debatable. An example of latent and sensible heat polynya is the ''North Water'' (NOW) polynya in northern Baffin Bay (Mysak and Huang 1992; DWM). However, the relative contribution of latent versus sensible heat in the maintenance of the NOW is still uncertain due to a lack of information about the seasonal circulation in the Baffin Bay.

DWM and DWS show that to simulate the shape of a coastal polynya it is important to take into account the frazil ice trajectories and, under certain circumstances, to include an accurate coastline. A consequence of this is that the modeled polynya ice edge does not necessarily follow the coastline, unlike the Pease (1987) and Ou (1988) models. A criterion is developed by DWS for determining whether a coastal feature will influence the steady-state shape of a coastal polynya. The authors derive an alongshore polynya adjustment length scale ($L^{(c)}$) in terms of the ''Lebedev–Pease width'' and the directions of drift of the frazil ice and the offshore consolidated thin ice. Coastline features with an alongshore length scale much smaller than $L^{(c)}$ will not be reproduced in the polynya ice edge.

However, a deficiency of the DWM and DWS studies is that frazil ice moves with prescribed constant velocity. This can be a serious shortcoming because in a large polynya, winds and oceanic currents are likely to have appreciable spatial variations. An immediate consequence of this is that the divergence of the frazil ice velocity field will be nonzero and, accordingly, the distribution of frazil ice inside the polynya will have a complicated structure. For example, if Langmuir cells are the dominant circulation within the polynya, the ice motion will have both along- and cross-wind components and the frazil ice will be approximately distributed in alternate bands of relatively high and low concentration (Martin and Kauffman 1981). In practice, the frazil ice in a polynya will be in approximately free-drift motion. Information about the wind stress and the upper-ocean circulation in the polynya is required to determine the frazil ice trajectories and, in combination with the production rate, the frazil ice distribution. This study presents a steady-state latent heat coastal polynya model in which the frazil ice trajectories are determined from the free-drift ice momentum balance, and the frazil ice depth is calculated from the balance between ice transport and ice production. Thus, the frazil ice distribution is in this model a fully prognostic variable, in contrast with DWM and DWS.

For simplicity, the consolidated thin ice transport is prescribed and it is assumed that the ice growth rate, the wind stress, and ocean circulation within the polynya are known. The model then determines the polynya ice edge. We focus here on the modeled size and shape of a latent heat coastal polynya for fixed forcing fields and analyze the sensitivity of the polynya ice edge to perturbations in those fields. Of course, the forcing fields are to a large extent coupled, and caution must be exercised when setting their distributions to ensure that they are not incompatible. For example, in the simulation of the Northeast Water polynya (NEW) presented in this paper we appeal to climatological information to define the forcing fields. Ideally, they could be derived from in situ observations or from the output of a coupled atmosphere–pack ice–ocean model. Alternatively, the polynya model could be embedded in a larger model including atmospheric, sea ice, and oceanic components in order to account for the interaction of the polynya with the local weather. We are developing a coupled model of this type.

The remainder of the paper is arranged as follows. Section 2 develops the model equations and the method used to solve them. The influence of wind and ocean currents on a polynya adjacent to an idealized straight coastline is discussed in section 3, for which analytical progress is possible. For a given coastline, wind stress, and ocean velocity field there is no guarantee that a closed coastal polynya will exist. Further, the choice of wind stress and ocean velocity field determines whether the polynya ice edge will exhibit a cusp. In section 3 both of these ideas are examined in the context of a wedge-shaped domain. In section 4 the model is used to simulate the early spring shape of the NEW polynya located between the Henrik Krøyer Islands (close to the mouth of Ingolfs Fjord) and the Ob Bank (a landfast ice shelf). This region is protected against ice import and is favorable for the formation of a wind-generated polynya in winter and early spring (Smith et al. 1990; Schneider and Budéus 1995; Minnett 1995). Finally, section 5 summarizes the key results.

2. The polynya model

Pease (1987) distinguishes three regions in the description of a latent heat coastal polynya. Proceeding from the coast offshore, these regions are (i) the region of open water with frazil ice, which is surrounded by (ii) the new to young ice region, which is in turn surrounded by (iii) the first-year ice region. Frazil ice is produced in region (i) and herded away from the coast by winds and oceanic currents, thus keeping the area open. The ocean circulation in this region frequently consists of Langmuir cells aligned with the wind or oriented at a certain angle to the right (in the Northern Hemisphere) of it. This angle can be of the order of 13° (Leibovich 1983). In practice, tidal motion, wind-driven, and buoyancy-driven currents will also exist within coastal polynyas. We are unaware of any published studies on the influence of these types of circulation on the development and maintenance of polynyas. The bound-

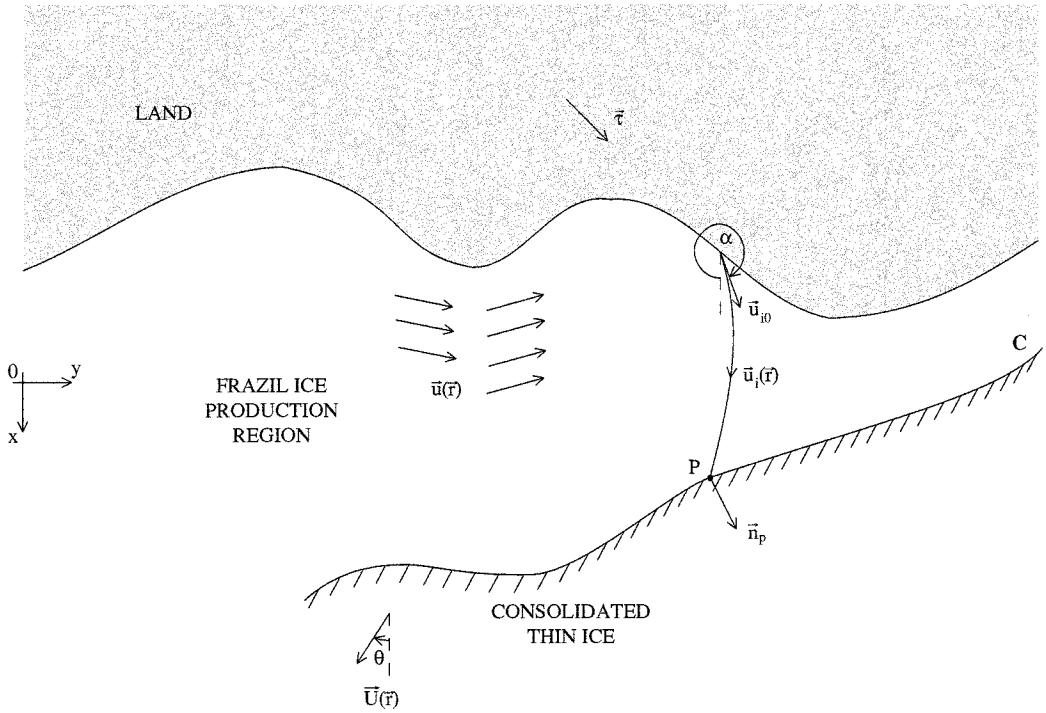

FIG. 1. Schematic diagram illustrating the polynya model. Any point P on the polynya ice edge C is determined so that the fluxes of frazil ice and consolidated ice balance across C. $\boldsymbol{\tau}$, $\mathbf{u}$, $\mathbf{u}_i$, and $\mathbf{U}$ denote the wind stress, the surface velocity of the ocean, the frazil ice velocity, and the consolidated thin ice velocity respectively. In general, all these fields depend on position. Also shown is the angle α between the initial point of a frazil ice trajectory and the x axis and the angle θ between the consolidated thin ice flux and the x axis.

ary between regions (i) and (ii) constitutes the polynya ice edge. In region (ii) the frazil ice consolidates into ice floes becoming thin new ice. The separation between regions (ii) and (iii) is the proper outer limit of the polynya. Pease (1987) assumes that the new ice in region (ii) and the first-year ice in region (iii) move away from the coast with the same velocity. This allows Pease (1987) to formulate a one-dimensional model for determining how the width of the polynya [i.e., region (i)] evolves in time.

Coastal polynyas are typically less than 100 km in width, which allows the use of a Cartesian coordinate frame (Fig. 1). The position vector of any point with respect to such frame is given by $\mathbf{r}$. We wish to determine the polynya ice edge C of a steady-state coastal polynya given the frazil ice production rate $F(\mathbf{r})$ (in units of m s^{-1}), the wind stress $\boldsymbol{\tau}$, the surface velocity field of the ocean $\mathbf{u}(\mathbf{r})$, the velocity $\mathbf{U}(\mathbf{r})$ of the consolidated thin ice and its thickness at the polynya ice edge $H(\mathbf{r})$, and the coastline shape. We must also specify one point on C, typically where the polynya ice edge intersects the coastline. In applications of the model to a particular polynya, the geometry of the coastline together with the direction of travel of the ice pack suggest the location of this point. As already mentioned, the surface oceanic velocity $\mathbf{u}(\mathbf{r})$ can have a complicated structure resulting from the interaction between wind, haline, and tidally driven flow. To investigate the combined effect of wind, haline, and tidally driven flow on the maintenance of a polynya, it would be appropriate to couple the polynya model to a numerical shelf circulation model (Blumberg and Mellor 1987). When applying the model to simulate a particular polynya, complicated behavior can result. To facilitate understanding of this behavior we analytically derive solutions of the model in an idealized case of a straight coastline with an alongshore current and a uniform wind stress that has both alongshore and offshore components.

We also note that it is not strictly necessary to have separate information about $\mathbf{U}(\mathbf{r})$ and $H(\mathbf{r})$ since our formulation only involves the variable $\mathbf{T}(\mathbf{r}) = H(\mathbf{r})\mathbf{U}(\mathbf{r})$, the consolidated thin ice transport. As pointed out by Pease (1987), the process of consolidation of frazil ice into ice floes at the polynya ice edge probably depends on the wind velocity and fetch, but its physics is not well known. In DWS the frazil ice trajectories were specified and $\mathbf{U}$ and H were assumed to be constant, in contrast with this study.

Following Pease (1987), the steady-state polynya ice edge is determined by requiring that there is a balance of fluxes of frazil and the consolidated thin ice across C. Referring to Fig. 1, the flux of frazil ice per unit length F_P across the polynya ice edge at point P is given by

$$F_P = D\mathbf{u}_i \cdot \mathbf{n}_P, \tag{1}$$

where $D(\mathbf{r}_P)$ is the frazil ice depth, $\mathbf{u}_i(\mathbf{r}_P) = (u_i(\mathbf{r}_P),$

$v_i(\mathbf{r}_P)$) is the frazil ice velocity, $\mathbf{r}_P$ is the position vector of P, and $\mathbf{n}_P$ is a unit normal to C at P. In contrast with DWS, $\mathbf{u}_i$ now depends on position. The consolidated thin ice transports a flux of ice per unit length I_P across C which at point P is given by

$$I_P = H\mathbf{U}\cdot\mathbf{n}_P. \tag{2}$$

The curve C is located where the fluxes (1) and (2) are equal, yielding a differential equation for the polynya ice edge that is given by

$$\frac{dx}{dy} = \frac{HU - Du_i}{HV - Dv_i}. \tag{3}$$

It is worth stressing at this point that D, $\mathbf{u}_i$, H, and $\mathbf{U}$ are functions of position, but in the special case when the frazil velocity and the consolidated thin ice depth and velocity are uniform, (3) reduces to the differential equation discussed in DWS. At this stage, (3) cannot be solved because D and $\mathbf{u}_i$ are unknown.

In a steady-state polynya, conservation of frazil ice requires that

$$\boldsymbol{\nabla}\cdot(\mathbf{u}_i D) = F, \tag{4a}$$

which upon expanding becomes

$$u_i\frac{\partial D}{\partial x} + v_i\frac{\partial D}{\partial y} = F - D\boldsymbol{\nabla}\cdot\mathbf{u}_i. \tag{4b}$$

Equation (4b) is readily solved for D using the method of characteristics. The characteristic curves are given by

$$\frac{dx}{dt} = u_i, \qquad \frac{dy}{dt} = v_i, \tag{5a}$$

and along these curves

$$\frac{dD}{dt} = F - D\boldsymbol{\nabla}\cdot\mathbf{u}_i, \tag{5b}$$

where t is a parameter (with units of time) along a characteristic.

Within the polynya the frazil ice trajectories are determined from the free-drift ice momentum balance

$$\rho_i f\mathbf{k}\times D\mathbf{u}_i = \boldsymbol{\tau}_{ia} - \boldsymbol{\tau}_{wi}, \tag{6}$$

where ρ_i denotes the ice density, $\mathbf{k}$ is a unit vector along the z axis (defined in such a way that the Cartesian reference frame is a right-handed one), and $\boldsymbol{\tau}_{ia}$ and $\boldsymbol{\tau}_{wi}$ denote the shear stress at the top and bottom of the ice respectively. Following Darby and Willmott (1993), the parameterization $\boldsymbol{\tau}_{wi} = \rho_i c_{wi}|\mathbf{u}_i - \mathbf{u}|(\mathbf{u}_i - \mathbf{u})$ is adopted, where c_{wi} is a constant water–ice drag coefficient. In this study, we prescribe $\boldsymbol{\tau}_{ia}$, and for notational convenience it will hereafter be denoted by $\boldsymbol{\tau}$. From (6) it is possible to analytically determine $\mathbf{u}_i$ in terms of $\mathbf{u}$, $\boldsymbol{\tau}$, and D, the details of which are given in appendix A. The system (3), (4b), and (6) can be solved for $\mathbf{u}_i$, D, and the polynya ice edge C provided that we know one point on C and using the condition that $D = 0$ on the coast.

Frazil ice is typically less than a few centimeters thick, and therefore the Coriolis term is normally much smaller than the shear stress terms in (6). For example, for wind velocities of $\sim$10 m s^{-1}, typical of the values reported by Pease (1987) for the St. Lawrence Island polynya in February, and oceanic currents of $\sim$0.1 m s^{-1}, the magnitude of the Coriolis term is less than 10% of the shear stresses for ice thinner than $\sim$0.4 m. This is true irrespective of the relative direction of the currents with respect to the wind. However, for completeness, the Coriolis term is retained in our formulation because, if regions exist where the frazil ice is convergent, D could be large enough [see (5b)] for this term to become significant. Of course, the assumption of uniform ice production is likely to be invalid where D exceeds, say, 0.3 m.

Given $\mathbf{u}$, $\mathbf{U}$, $\boldsymbol{\tau}$, and F, Eqs. (3), (4b), and (6) are solved in the following manner. Suppose the solution procedure has determined the points $(x_p^{(i)}, y_p^{(i)})$ on C for $i = 1, \ldots, N-1$ and we wish to calculate $(x_p^{(N)}, y_p^{(N)})$. In appendix A it is shown how $\mathbf{u}_i$, and hence $\boldsymbol{\nabla}\cdot\mathbf{u}_i$, can be obtained in terms of $\boldsymbol{\tau}$, $\mathbf{u}$, and D. To advance C to $(x_p^{(N)}, y_p^{(N)})$ a fourth-order Runge–Kutta scheme is used to integrate (3), but in order to do this we need D at intermediate points. Wherever D is required, an estimated value is first chosen (based on the closest known value) and system (5) is integrated along a frazil ice trajectory until the coastline is intersected where, in general, D will be nonzero. The initial estimate for D is refined and the procedure is repeated until a solution is obtained that differs from zero on the coastline by less than a specified tolerance.

3. Polynya solutions with idealized coastlines

In this section, analytical results for the polynya width are derived when the coastline is straight, provided that $\boldsymbol{\tau}$, $\mathbf{u}$, and F are uniform in the alongshore direction. We next analyze the polynya shape as a function of the prescribed uniform wind stress and consolidated ice transport in a wedge-shaped domain in which the ocean velocity field is nondivergent and irrotational. The wedge problem exhibits a number of interesting features that can occur in real-world applications of the model. In both examples, we assume that the consolidated ice transport $H\mathbf{U}$ is spatially uniform. These examples will help us to understand in simple terms how the structure of the frazil ice trajectories influences both the size and shape of the polynya, and to interpret the results obtained in the application of the model to the NEW polynya in section 4.

a. Straight coastline

Consider the case when the coastline coincides with the y axis and the ocean occupies the region $x > 0$. Although $\boldsymbol{\tau}$, $\mathbf{u}$, and F are assumed to be uniform in the alongshore direction, no restriction is placed on the off-

shore spatial dependence of these fields. Clearly $\mathbf{u}_i$ and D only depend on x and (4a) reduces to

$$\frac{d(u_i D)}{dx} = F. \tag{7}$$

Suppose the polynya intersects the coastline. In practice, the intersection point is determined from the shape of the coast and the pack ice drift. Where the polynya intersects the coastline in this example could be viewed as the limit of a fast ice barrier. Integrating (3) from this point will yield a curve C that asymptotes along the line $x = L^{(p)}$, where

$$HU = \int_0^{L^{(p)}} F\, dx = (u_i D)|_{x=L^{(p)}}, \tag{8}$$

upon integrating (7). Thus, the asymptotic polynya width $L^{(p)}$ depends only on the offshore flux of consolidated thin ice, which is trying to open the polynya, and the total frazil ice production rate per unit length in the alongshore direction, which is trying to close the polynya: $L^{(p)}$ does not depend explicitly upon the detailed structure of the frazil ice trajectories, although it does, in general, depend on the frazil ice depth via F. However, since the frazil ice concentration and depth within the polynya are relatively low, F can be regarded as being approximately independent of the frazil ice distribution. Pease (1987) suggests that the steady-state polynya width is not controlled by the wind because to a good approximation $\mathbf{U}$ and F vary near linearly with $|\boldsymbol{\tau}|$. Equation (8) shows that this is still the case in two dimensions. If the frazil ice production is constant within the polynya, (8) leads to $L^{(p)} = (HU)/F$, which is the Lebedev–Pease steady-state width.

Contrary to $L^{(p)}$, the alongshore length scale $L^{(c)}$ over which the polynya adjusts toward its asymptotic width does depend upon the frazil ice trajectories. In DWS the definition of $L^{(c)}$ exploited the fact that the frazil ice trajectories were a family of parallel straight lines, which is not, in general, the case here. We therefore consider an alternative definition for $L^{(c)}$, which reduces to that in DWS under the assumptions made by these authors. The tangent to C at a point $P = (x_P, y_P)$ intersects the line $x = L^{(p)}$ at the point $Q = (L^{(p)}, y_Q)$, where $y_Q = s(L^{(p)} - x_P) + y_P$ and $s = (dy/dx)|_{(x_P, y_P)}$. Now define

$$L^{(c)} = \lim_{x_P \to L^{(p)}} |s(L^{(p)} - x_P)|. \tag{9}$$

If the polynya width at P is sufficiently close to $L^{(p)}$, the length of the interval parallel to y within which a linear approximation to C is valid is $|s(L^{(p)} - x_p)|$. Unlike $L^{(p)}$, the length scale $L^{(c)}$ depends on $\mathbf{u}$ and $\boldsymbol{\tau}$ via the slope s of the polynya ice edge.

To make analytical progress beyond this point and to facilitate understanding about $L^{(p)}$ and $L^{(c)}$ it is necessary to introduce further simplifying assumptions. For example, we can eliminate the Coriolis term in the ice momentum balance (6) on the basis that the depth of frazil ice is generally small enough to make this term negligible compared with the shear stress terms. The frazil ice velocity field is then independent of the frazil ice depth and it is given by

$$\mathbf{u}_i = \mathbf{u} + \boldsymbol{\tau}(\rho_i c_{wi} |\boldsymbol{\tau}|)^{-1/2}. \tag{10}$$

In this case, it is straightforward to derive the following expression for the slope of the polynya ice edge, namely,

$$\frac{dx}{dy} = \frac{HU - \displaystyle\int_0^x F(x')\, dx'}{HV - \dfrac{v_i}{u_i} \displaystyle\int_0^x F(x')\, dx'}. \tag{11}$$

Notice that the right-hand side of (10) is a function of x alone so that (11) can, in principle, be integrated to obtain C. As an illustration, consider the case when $\mathbf{u}$ is an alongshore current with offshore shear and $\boldsymbol{\tau}$ and F are spatially uniform. Let the oceanic velocity be given by

$$u = 0, \qquad v = v_0 + \mu x, \tag{12}$$

where μ is a constant. Integrating (11), the polynya ice edge passing through the origin is given by

$$\begin{aligned} y = {} & L^{(p)}\{\tan\theta - \tan\alpha + L^{(p)}\mu(|\mathbf{u}_{i0}| \cos\alpha)^{-1}\} \\ & \times \ln\left(1 - \frac{x}{L^{(p)}}\right) - \{\tan\alpha - L^{(p)}\mu(|\mathbf{u}_{i0}| \cos\alpha)^{-1}\}x \\ & + \frac{1}{2}\mu(|\mathbf{u}_{i0}| \cos\alpha)^{-1}x^2, \end{aligned} \tag{13}$$

where $\mathbf{u}_{i0}$ is the velocity of the frazil ice at the coast and the angles α and θ define the directions of $\mathbf{u}_{i0}$ and $\mathbf{U}$, respectively, and increase in the clockwise direction from the x axis. The length scale $L^{(c)}$ in this case becomes

$$L^{(c)} = L^{(p)}|\tan\alpha - \tan\theta - L^{(p)}\mu(|\mathbf{u}_{i0}| \cos\alpha)^{-1}|. \tag{14}$$

Expressions (13) and (14) reduce to (8) and (9) in DWS when $\mu = 0$. If either the coastal frazil ice or the consolidated thin ice travel almost parallel to the coastline, the alongshore adjustment scale (14) will be large. On the other hand, if the coastal frazil ice and the consolidated thin ice travel in similar directions, $L^{(c)}$ can still be large if $L^{(p)}\mu|\mathbf{u}_{i0}|$ is large. Alongshore spatial variations in the coastline or in the atmospheric and oceanic forcing fields that are much smaller than $L^{(c)}$ will have negligible effect on the shape of the polynya ice edge.

Figure 2 shows plots of the polynya ice edge (13) for three values of μ when $\boldsymbol{\tau}$ and F are fixed. In Fig. 2 $\boldsymbol{\tau} = 0.025(\cos(26°), \sin(26°))$ N m^{-2}, $|H\mathbf{U}| = 0.015$ m^2 s^{-1}, $\theta = 25°$, $F = 0.04$ m d^{-1}, and $v = 0.1 + \mu x$ m s^{-1}. Note that while the asymptotic polynya width ($\sim$28 km) is unaffected by the offshore shear of the oceanic velocity field, as implied by (8), the frazil ice trajectories and transport are sensitive to this quantity. Therefore, in the region where the polynya adjusts to its asymptotic width the shape of C is sensitive to the value of μ. The

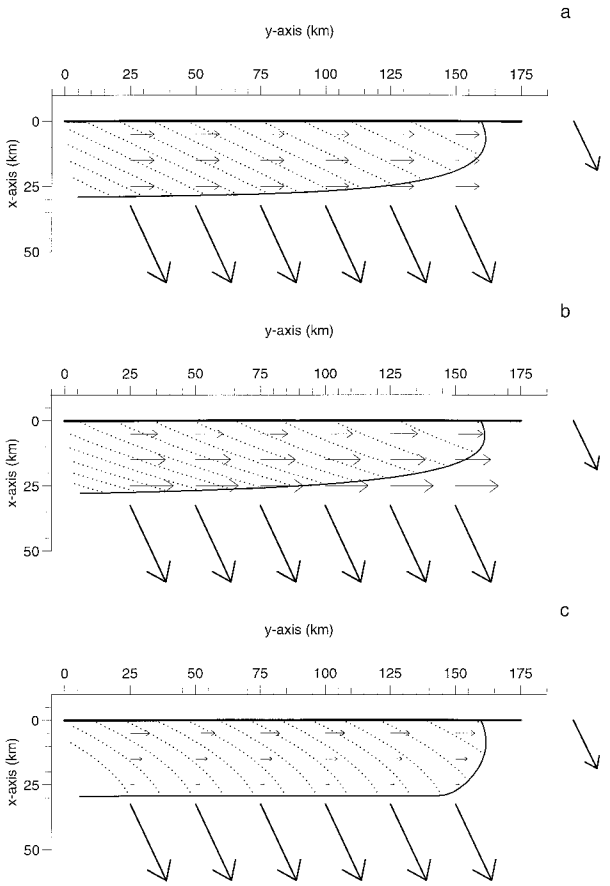

FIG. 2. The polynya solution (16), with the origin shifted 160 km along the x axis, for $\mu = 0$ (a); $\mu = 0.33 \times 10^{-5}$ s^{-1} (b); and $\mu = -0.33 \times 10^{-5}$ s^{-1} (c). The bold arrow on the y axis indicates the direction of the wind stress. The arrows within the polynya correspond to the direction and relative magnitude of the oceanic currents. The length and direction of the heavy arrows on the consolidated thin ice denote the Lebedev–Pease width L ($L = H|\mathbf{U}|/F$) and the direction of motion of the consolidated ice, respectively. The dotted lines crossing the polynya correspond to selected frazil ice trajectories. The heavy continuous line indicates the location of the polynya ice edge.

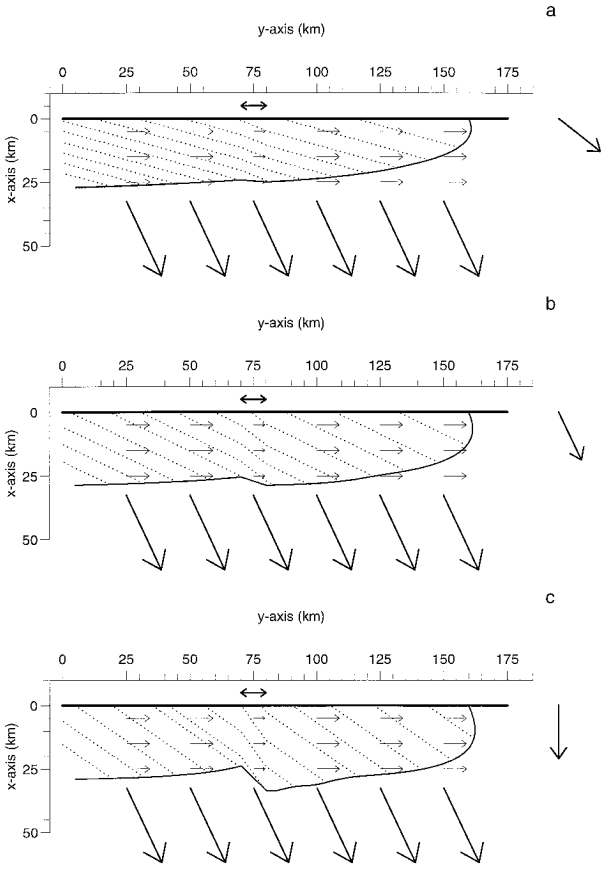

FIG. 3. Numerical polynya ice edge solutions for a nonuniform alongshore oceanic current with $\theta_a = 52°$ (a), $\theta_a = 26°$ (b), and $\theta_a = 0°$ (c); $H\mathbf{U}$ and F are as in Fig. 2.

alongshore extent of this region is approximately given by $L^{(c)}$ in (14). In Figs. 2a, 2b, and 2c the alongshore length scale is $L^{(c)} = 92$, 130, and 9 km, respectively. Since the coastline expands indefinitely to the left, the polynya can always attain its asymptotic width. Of course, in reality the coastline is finite and its length is approximately an upper bound to the alongshore extent of the polynya. If the coast is 50 km long, say, the actual polynya will never reach its asymptotic width when $L^{(c)}$ is significantly larger than 50 km. The importance of the alongshore adjustment length $L^{(c)}$ is also demonstrated in Fig. 3, in which F is the same as in Fig. 2 and $f = 0$. Again $\mathbf{u}$ is parallel to the coast, but it is now piecewise uniform in the alongshore direction with

$$v(y) = \begin{cases} v_1, & y \le y_l, y_r \le y \\ v_2, & y_l \le y \le y_r. \end{cases}$$

The polynya ice edge C is numerically determined when the wind stress has fixed magnitude but varying offshore direction. Figures 3a–c show solutions of this problem for $\boldsymbol{\tau} = 0.025(\cos(\theta_a), \sin(\theta_a))$ N m^{-2}, with an alongshore oceanic current given by $v = 0.1$ m s^{-1}, except in the region 70 km $\le y \le$ 80 km, indicated by a bold, double headed arrow, where $v = 0.05$ m s^{-1}. From (14) it is clear that varying the direction of $\boldsymbol{\tau}$ leads to a change in $L^{(c)}$ through the angle α and $|\mathbf{u}_{i0}| \cos\alpha$. As $\boldsymbol{\tau}$ rotates from an alongshore (see Fig. 3a) to an offshore direction (see Fig. 3c), $L^{(c)}$ decreases. In Fig. 3a the polynya ice edge shows little change in the region $y_l \le y \le y_r$ because $L^{(c)} = 92$ km $\gg y_r - y_l = 10$ km. However, in Fig. 3c the polynya ice edge changes orientation significantly in (y_l, y_r) because $L^{(c)} = 28$ km. The alongshore length scale in Fig. 3b is 47 km. There is an analogy between the results in Fig. 3 and those in DWS for the influence of a bay or headland on a polynya ice edge, where the alongshore length scale of the coastal feature plays the role of the length scale $y_r - y_l$. Perturbations in the wind field, the production rate of frazil ice and the consolidated thin ice transport will also lead to modifications in the polynya shape depending on

whether the size of the region where the perturbation takes place is large or small compared with $L^{(c)}$.

With the reintroduction of the Coriolis term in the ice momentum balance, the solutions in Figs. 2 and 3 show imperceptible changes, and this is consistent with the fact that the frazil ice depths remain shallow within the polynya region.

b. Wedge-shaped domain

In this example the ocean is contained within the wedge-shaped domain bounded by the straight lines $y = px$ (line R_1) and $x = py$ (line R_2) where the constant p satisfies $|p| \leq 1$. This case illustrates the generic behavior of the polynya in an embayment. We suppose that $\boldsymbol{\tau}$, F, and $H\mathbf{U}$ are uniform and that the ocean velocity field is given by

$$\mathbf{u} = \mathbf{k} \times \nabla\Psi, \tag{15a}$$

where the streamfunction Ψ is given by

$$\Psi = C(y - px)(x - py), \tag{15b}$$

where C is an arbitrary positive constant. Clearly, $\mathbf{u}$ is irrotational and nondivergent and, although $|\mathbf{u}|$ grows without bound as $r \to \infty$, the behavior of the model in the neighborhood of the origin exhibits many interesting features that could be reproduced when simulating a polynya.

For analytical progress we again assume that the Coriolis term in (6) is negligible, and in this case it is straightforward to show that the upstream (downstream) asymptotic frazil ice velocity is oriented parallel to R_1 (R_2) and that at any point $P = (x, y)$ the component of $\mathbf{u}_i$ normal to R_1 (R_2) is solely a function of the distance from P to R_1 (R_2). Upon integration of (10), the parametric form of the frazil ice trajectories is given by

$$x = \frac{1}{C(1 - p^2)^2(\rho_i c_{wi}|\tau|)^{1/2}}((1 + p^2)\tau^x - 2p\tau^y) + pA_1e^{C(1-p^2)t} + A_2e^{-C(1-p^2)t} \tag{16a}$$

$$y = \frac{1}{C(1 - p^2)^2(\rho_i c_{wi}|\tau|)^{1/2}}(2p\tau^x - (1 + p^2)\tau^y) + A_1e^{C(1-p^2)t} + pA_2e^{-C(1-p^2)t}, \tag{16b}$$

where the constants A_1 and A_2 determine the starting point of the trajectory and $\boldsymbol{\tau} = (\tau^x, \tau^y)$, and t is time along a trajectory. Elimination of t between (16a) and (16b) shows that the frazil ice trajectories are the family of hyperbolas

$$\left\{(px - y) + \frac{p\tau^x - \tau^y}{C(1 - p^2)^2(\rho_i c_{wi}|\tau|)^{1/2}}\right\} \times \left\{(py - x) - \frac{p\tau^y - \tau^x}{C(1 - p^2)^2(\rho_i c_{wi}|\tau|)^{1/2}}\right\} = (1 - p^2)^2A_1A_2. \tag{17}$$

The asymptotes of (17) are a pair of straight lines parallel to R_1 and R_2. Let Q_1 and Q_2 denote these asymptotes, with Q_j parallel to R_j ($j = 1, 2$). Then Q_j intersect at the point (q_1, q_2), where

$$q_1 = \frac{(1 + p^2)\tau^x - 2p\tau^y}{C(1 - p^2)^3(\rho_i c_{wi}|\boldsymbol{\tau}|)^{1/2}}$$

$$q_2 = \frac{2p\tau^x - (1 + p^2)\tau^y}{C(1 - p^2)^3(\rho_i c_{wi}|\boldsymbol{\tau}|)^{1/2}}. \tag{18}$$

Three physically distinct regimes can now be identified based on the location of (q_1, q_2) and are illustrated for the case of a quarter plane where $p = 0$.

Case A: $\quad -\tau^x + p\tau^y > 0, \qquad p\tau^x - \tau^y < 0. \tag{19}$

In this case, Q_1 and Q_2 are outside the oceanic domain and the frazil ice trajectories can only emanate from the boundary R_1. Physically this occurs because the normal component of wind stress on R_2 is out of the ocean domain [first inequality (19)], while the normal component of wind stress on R_1 is into the domain [second inequality (19)]. On R_1 the oceanic flow is directed along the boundary, and we therefore require the normal component of wind stress on this boundary to be directed into the domain if frazil ice trajectories are to leave R_1. Figure 4a shows a plot of the frazil ice trajectories together with two polynya solutions corresponding to two distinct starting points on R_1. In the numerical computation of these solutions (and of the others presented in this section) the Coriolis term in (6) has been retained, and the oceanic currents (not shown) have been derived from (15) with $C = 7.4 \times 10^{-7}$ s^{-1}, and $H\mathbf{U}$ and F the same as in Fig. 2. Therefore, the frazil ice trajectories shown here approximately coincide with those given in (17) when the Coriolis term in (6) is small (i.e., sufficiently close to the wedge angle). Note that the polynya solutions asymptote to a uniform width despite that the magnitude of the ocean velocity field increases without bound with increasing distance from the corner along R_1. For completeness we analyze the asymptotic behavior of the polynya far from the corner in appendix B.

Case B: $\quad -\tau^x + p\tau^y < 0, \qquad p\tau^x - \tau^y > 0. \tag{20}$

Both Q_1 and Q_2 traverse the ocean domain with the normal component of wind stress on R_2 now directed into the domain, while that on R_1 is out of the domain. It can be shown using (20) that (q_1, q_2) lies inside the ocean domain in this case. Frazil ice trajectories can only emanate from R_2. An example of the frazil ice trajectories for this case is shown in Fig. 4b. The asymptotes Q_1 and Q_2 are shown as bold dotted lines. As the length of a trajectory increases so, too, does the frazil ice depth and velocity, and the Coriolis term becomes significant in (6). Thus, the trajectories deflect to the right in the sense of the motion and do not asymptote along the line Q_2. They do, however, asymptote to a line that forms an acute angle with the x axis.

A singular point (S, say) in the ocean domain exists

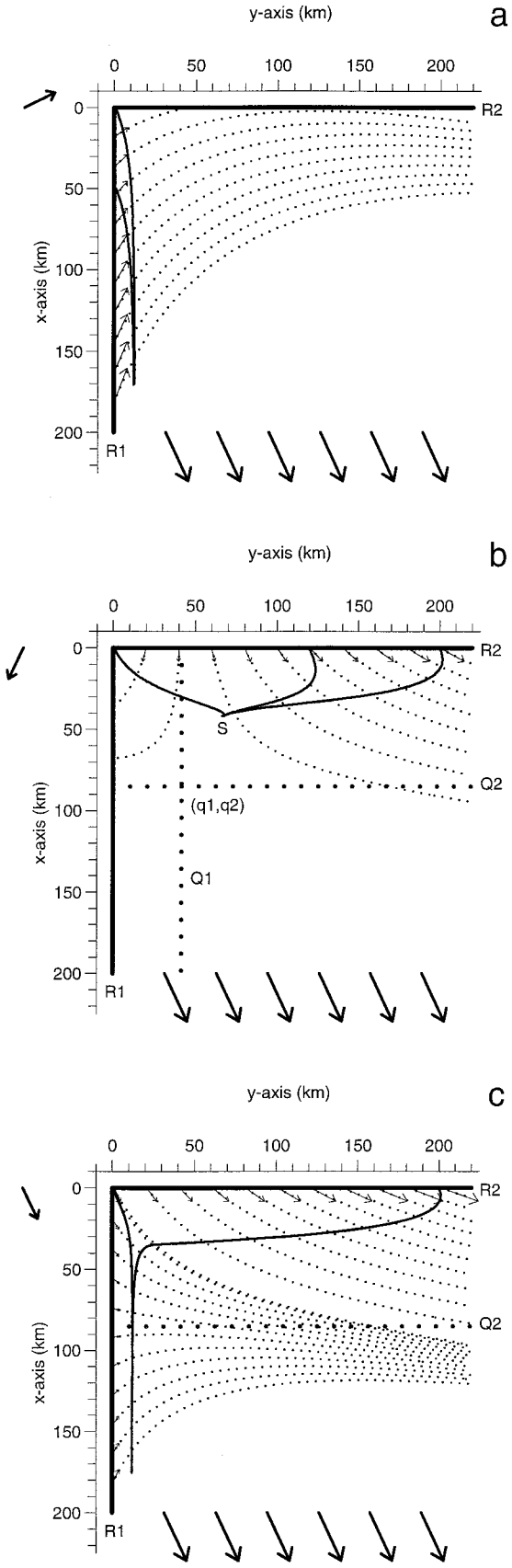

where the frazil ice transport and the consolidated ice transport are equal. At S both the numerator and the denominator of the right-hand side of (3) vanish and *all* polynya ice edge curves pass through this point. Figure 4b shows the polynya ice edge starting at the origin and terminating at S. Two further polynya ice edge curves starting on R_2 are also plotted in Fig. 4b. The resulting closed coastal polynya has a cusp at S. This feature is most probably of minor physical importance but it shows that the polynya ice edge can exhibit discontinuities in its slope that are not linked with either the geometry of the coast or with abrupt spatial changes in the forcing fields.

Case C: $$-\tau^x + p\tau^y < 0, \qquad p\tau^x - \tau^y < 0. \tag{21}$$

Only Q_2 traverses the ocean domain and the normal component of wind stress on both R_1 and R_2 is into the domain, which can be seen immediately from (21). Frazil ice trajectories can start at any point on R_1 or R_2. Figure 4c shows plots of this type of solution with the asymptote Q_2 shown as a bold dotted line. As in Fig. 4b the influence of rotation leads to the trajectories asymptoting to a straight line that is tilted with respect to Q_2. Two polynya solutions are also shown in Fig. 4c. A ''single branch'' polynya will occur provided that a point on R_1 is chosen as the initial condition. When (3) is integrated from any point on R_2, a ''double branch'' polynya results. Far from the corner the single and double branch solutions asymptote to uniform widths (distinct for each branch) despite that the alongshore ocean velocity field is nonuniform. This property is also exhibited in Fig. 4a.

If the normal components of wind stress on R_1 and R_2 are directed away from the ocean domain [corresponding to reversing the inequalities (21)], no polynya is possible since the frazil ice will be flowing from the domain interior toward the coastal boundaries.

4. Application to the Northeast Water polynya

The Northeast Water polynya (NEW) occurs over the continental shelf off the northeast coast of Greenland. Schneider and Budéus (1995) conclude that the NEW is formed due to the interaction of a fast ice barrier extending perpendicular from the coast and a northward flowing coastal current. The region downstream of the

←

FIG. 4. Numerical solutions of the polynya ice edge problem in a quarter-plane domain for $\boldsymbol{\tau} = 0.025(\cos(\theta_a), \sin(\theta_a))$ N m^{-2} with $\theta_a = 116°$ (a), $\theta_a = -26°$ (b), and $\theta_a = 26°$ (c); $H\mathbf{U}$ and F are as in Fig. 1. Numerically determined frazil ice trajectories have been plotted as light dotted lines starting in the coastlines $y = 0$ (R_1) and/or $x = 0$ (R_2). The light arrows at the beginning of the trajectories indicate the direction and relative velocity of the frazil ice at that point. The heavy dotted lines correspond to the asymptotes Q_1 and Q_2. Two polynya solutions (heavy continuous line) are shown in each case.

barrier is protected from ice import while current-driven ice export continues. However, the authors point out that the area between the Henrik Krøyer Islands and the Ob Bank is favorable for wind-generated polynyas throughout the winter because these coastal features prevent direct ice import into the region. Minnett (1995) also supports this observation. Infrared and satellite images reveal that in the winter, open water frequently occurs close to the coast at the northern part of the polynya, which is associated with northwesterly winds blowing the ice from the coast (Minnett 1995).

We apply the model to the NEW region to simulate the wind-driven coastal polynya that occurs in winter and early spring. In addition, the sensitivity of the polynya shape to the oceanic circulation, wind stress, ice production rate, and consolidated ice flux are examined.

The digital coastline data was provided by M. Johnson (1995, personal communication) and is plotted in Fig. 5. The bold broken lines represent the boundary of landfast ice present during winter and early spring (Schneider and Budéus 1995). Over the East Greenland Sea shelf an anticyclonic circulation exists (Budéus and Schneider 1995; Johnson and Niebauer 1995). To model this circulation a velocity streamfunction Ψ_I, (x, y) is defined for the interior flow, away from the coastline, in terms of which the interior ocean velocity field is given by

$$\mathbf{u}_I = \mathbf{k} \times \nabla\Psi_I. \tag{22}$$

The form of Ψ_I is given by

$$\Psi_I^2 = \left(\frac{x\cos\lambda - y\sin\lambda - \hat{a}_1}{a_2}\right)^2 + \left(\frac{x\sin\lambda + y\cos\lambda - \hat{b}_1}{b_2}\right)^2, \tag{23a}$$

where

$$\hat{a}_1 = a_1\cos\lambda - b_1\sin\lambda, \qquad \hat{b}_1 = a_1\sin\lambda + b_1\cos\lambda \tag{23b}$$

and a_1, b_1, and λ are constants. Streamlines are a family of confocal ellipses centered at $(\hat{a}_1, \hat{b}_1)$ with major and minor axes of length proportional to $2a_2$ and $2b_2$ respectively. When $\lambda = 0$, the major and minor axes coincide with the x axis and y axis respectively.

Clearly, $\mathbf{u}_I$ calculated from (22) and (23) does not satisfy the boundary conditions of no-normal flow and no slip at the coastline. A streamfunction $\Psi(x, y)$ can be calculated that satisfies the former boundary condition and takes the form of (23) in the ocean interior by demanding that Ψ satisfies the boundary value problem

$$r\nabla^2\Psi + \Psi_x = \Psi_{Ix}, \tag{24}$$

with $\Psi = 0$ on all rigid boundaries of the domain. In (24), r is a constant that can be thought of as a bottom friction parameter. The computational domain of (24) is contained within a rectangle of dimensions 2000 km × 600 km centered at (79.3°N, 13°W). The boundaries for the integration of (24) consist of the Greenland coastline contained within the rectangle together with those portions of the rectangle's sides that are contiguous to oceanic points. The width of the frictional coastal boundary layer is $O(r)$ and is chosen to be 2.5 km, and the method of successive overrelaxation is used to solve (24).

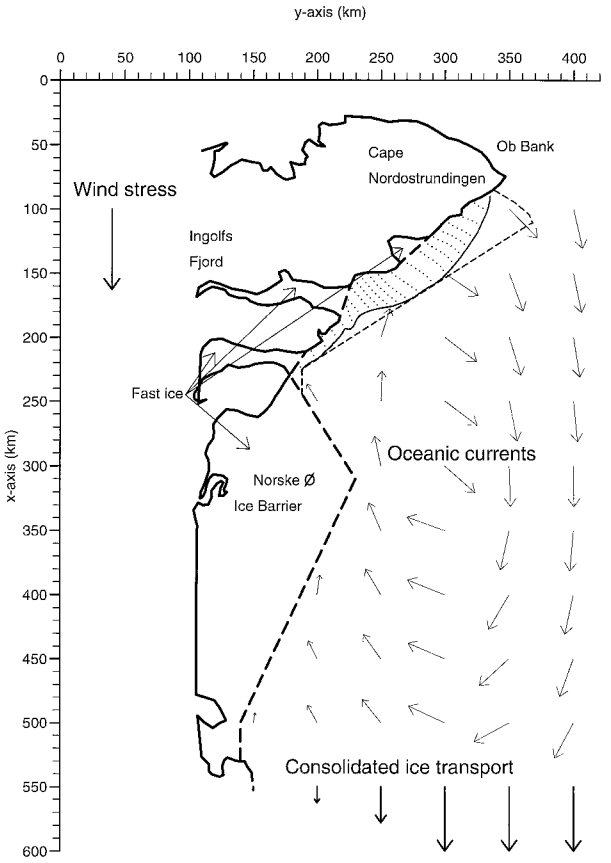

FIG. 5. The control solution for the NEW polynya (experiment 1). The point (0 km, 100 km) approximately corresponds to (82.1°N, 21°W). Also plotted is the coastline together with idealized landfast ice boundaries (bold dashed lines). Selected frazil ice trajectories are denoted by dotted lines within the polynya. The thin dashed line is the contour of a polynya observed on 6 May 1991 (redrawn from Norske Meteorologiske Institutt 1991).

The ocean velocity field $\mathbf{u}$ is calculated using (22) with Ψ_I replaced by Ψ. Finally, to ensure that the magnitude of the velocity field is realistic, $|\mathbf{u}|$ is normalized to a value of 0.125 m s^{-1} (Johnson and Niebauer 1995). Parameter values used for the standard run are listed in Table 1. To the best of our knowledge, no complete climatology of the atmospheric and oceanic conditions in the region of the NEW polynya is available. To define realistic values for the winter surface wind stress and frazil ice production in the NEW we have used a monthly mean climatology of surface air temperatures, dewpoint, sea level pressure, surface winds, and cloud cover from which bulk surface heat and momentum fluxes

TABLE 1. List of parameters for the standard run.

Parameter	Description	Value
a_1	Interior streamfunction parameter	-440×10^3 m
b_1	Interior streamfunction parameter	200×10^3 m
a_2	Interior streamfunction parameter	6 m
b_2	Interior streamfunction parameter	3 m
λ	Interior streamfunction parameter	$-10°$
$\|\boldsymbol{\tau}\|$	Magnitude of the wind stress	0.09 N m^{-2}
θ_a	Wind stress direction[a]	0
$\|\mathbf{u}\|$	Magnitude of the oceanic currents[b]	0.125 m s^{-1}
$\|H\mathbf{U}\|$	Magnitude of the consolidated ice transport[c]	0.02 m^2 s^{-1}
θ_{ci}	Consolidated ice transport direction[a]	0
F	Frazil ice production	0.04 m day^{-1}
c_{wi}	Ice–ocean drag coefficient	5.5×10^{-3}

[a] Angles are given with respect to the x axis and increase in the clockwise direction.
[b] $|\mathbf{u}|$ linearly decays to 0 in the region $0 \le y \le 200$ km (see Fig. 5).
[c] $|H\mathbf{U}|$ quadratically decays to 0 in the region 0 km $\le y \le$ 200 km (see Fig. 5).

TABLE 2. Estimated surface fluxes at (79.5°N, 12.5°W).*

Variable	Unit	Apr	May
Incoming shortwave radiation	W m^{-2}	106	187
Incoming longwave radiation	W m^{-2}	176	238
Outgoing longwave radiation	W m^{-2}	301	301
Sensible heat	W m^{-2}	−240	−37
Latent heat	W m^{-2}	−84.0	−29
Net heat flux	W m^{-2}	−344	59
Frazil ice production	m day^{-1}	0.1	−0.02
Wind stress magnitude	N m^{-2}	0.1	0.08
Wind stress direction	°N	178	−179

* Surface air temperature is −20°C in April and −10°C in May. Sea surface temperature is −2.8°C.

have been computed at the geographical location (79.5°N, 12.5°W), which is the closest point to the NEW in the data, slightly to the south of the observed polynya. Both the climatology and the bulk formulae employed in the derivation of the surfaces fluxes are documented in Fichefet and Morales Maqueda (1997). Table 2 lists the radiative, sensible, and latent heat and mechanical surface fluxes obtained for April (late winter) and May (early spring) at this location. The frazil ice production F is simply the net surface heat flux divided by the latent heat of fusion of ice. In Table 1 the values of F and $\boldsymbol{\tau}$ represent the average of the April and May estimates.

Note that the consolidated thin ice transport $\mathbf{T}$ is a free parameter in this formulation of the model. The value chosen for $\mathbf{T}$ in the control run has been derived by assuming a consolidated thin ice thickness of 0.2 m and a southward ice drift of 0.1 m s^{-1} (Emery et al. 1991). A more realistic simulation could be obtained by calculating $\mathbf{T}$ as a function of the wind stress and oceanic currents. However, to do so would require the use of a model for the motion (and possibly the growth) of consolidated thin ice. Ideally, the pack ice momentum balance equation should include an explicit representation of the internal ice stresses, which are likely to be large in this region. Alternatively, it would be possible to employ the linear relationship between ice motion and wind and oceanic currents derived by Thorndike and Colony (1982) for ice motion in the central Arctic. However, as these authors acknowledge, this empirical law works poorly in the northern Greenland Sea ice pack.

Table 3 lists the sensitivity experiments discussed below and, with the exception of experiments 5, 6, and 10, includes the value of the single parameter that has been varied from the control run. Of course, varying one parameter or field while leaving the others unchanged is unphysical because most, if not all of them, are interrelated. However, this is in the spirit of all sensitivity studies. In the control experiment we have used a realistic scenario of meteorological and oceanic conditions from which to compute the polynya solution. Nevertheless, our choice of forcing fields is certainly not unique. We believe that the forcing fields imposed in the sensitivity experiments are equally plausible for the NEW region as those defined in the control experiment. In all the experiments, the polynya ice edge has been integrated from the initial point (81.3°N, 12°W) on the eastern tip of Cape Nordostrundingen, where the polynya is usually observed to intersect the coast (e.g., Schneider and Budéus 1995). However, the precise coordinates of the starting point are to some extent arbitrary in the sense that closed polynya solutions can be obtained starting from points on this cape either to the east or to the west of the chosen starting point. We return to this point in experiment 10.

Experiment 1: Standard run. Figure 5 shows the coastal polynya for a equatorward wind stress. The ocean and ice velocity vectors are plotted. In the western part of the domain, the oceanic currents flow against the wind, and we therefore expect that the magnitude of the consolidated thin ice transport to decrease upon approaching the coast, as indicated by our choice of $\mathbf{U}$. The maximum polynya width is approximately 30 km [which agrees well with the estimate given by (8)], and its area is approximately 4200 km^2 (Table 4 lists the area occupied by the polynya solutions in the sensitivity experiments). Within the polynya the dotted lines represent the frazil ice trajectories. The maximum frazil ice depths (~0.15 m) occur at the ice edge roughly in the central part of the polynya. In this region, the northeastward oceanic currents slow down the advance of the frazil toward the polynya ice edge leading to a large residence time of frazil ice in open water (around 3.5 days). Also included in Fig. 5 is the approximate location of a polynya ice edge observed in the NEW region on 6 May 1991 (Norske Meteorologiske Institutt 1991). The northeastern boundary of the polynya is formed by fast ice on Ob Bank (not shown). The observed and simulated polynyas have similar alongshore and offshore extents. Detailed comparison, however, is inappropriate because we cannot be sure whether the

TABLE 3. A summary of the sensitivity experiments.

Experiment	Description	Parameter change
1	Standard run	See Table 1
2	Varying the wind stress magnitude	
a		$\|\boldsymbol{\tau}\| = 0.125$ N m^{-2}
b		$\|\boldsymbol{\tau}\| = 0.075$ N m^{-2}
c		$\|\boldsymbol{\tau}\| = 0.050$ N m^{-2}
d		$\|\boldsymbol{\tau}\| = 0.025$ N m^{-2}
3	Varying the wind stress direction*	
a		$\theta_a = +15°$
b		$\theta_a = -15°$
c		$\theta_a = -30°$
d		$\theta_a = -45°$
4	Varying the magnitude and direction of the consolidated ice flux*	
a		$\|H\boldsymbol{U}\| = 0.03$ m^2 s^{-1}
b		$\|H\boldsymbol{U}\| = 0.01$ m^2 s^{-1}
c		$\theta_{ci} = -10°$
d		$\theta_{ci} = +10°$
5	Varying the frazil ice production	
a		$F = 0.06$ m day^{-1}
b		$F = 0.05$ m day^{-1}
c		$F = 0.03$ m day^{-1}
d		$F = 0.02$ m day^{-1}
6	Varying the frazil ice production given by (25)	
a		$T_a = -22°$ C (F (0) $= 0.04$ m day^{-1})
b		$T_a = -32°$ C (F (0) $= 0.06$ m day^{-1})
c		$T_a = -12°$ C (F (0) $= 0.02$ m day^{-1})
7	Varying the ice–ocean drag coefficient	$0.0045 \leq c_{wi} \leq 0.0065$
8	Influence of land fast ice	
9	Varying the ocean circulation	
a		$-10° \leq \lambda \leq 10°$
b		$a_2/b_2 = 1.5$
c		$\|\boldsymbol{u}\| = 0$
10	Varying the starting point of the polynya	
11	Consolidated thin ice flux depending on wind and currents	
a		$\boldsymbol{T}$ calculated as in Thorndike and Colony (1982)
b		$\boldsymbol{T}$ calculated via the free-drift momentum balance

* Angles are given with respect to the x axis and increase in the clockwise direction.

prevailing meteorological conditions at the moment of observation are comparable to those used in deriving our forcing fields.

Experiment 2: Varying the wind stress magnitude. The polynya shape is insensitive to the magnitude of the northerly wind stress, which is consistent with the results in section 3a, where it is shown that for fairly uniform alongshore conditions the polynya width depends only on the consolidated ice transport and frazil ice production. Note that the frazil ice trajectories become more aligned with the oceanic coastal flow as $|\boldsymbol{\tau}|$ decreases, which is seen by comparing Figs. 6a to 6d. Since in Fig. 6d the length of the trajectories increases and the frazil ice velocity decreases, the frazil ice depth at the polynya ice edge increases. Maximum depths in experiment 2d are ~0.4 m east of Ingolfs Fjord, corresponding to a residence time of about 10 days. However, the component of $\mathbf{u}_i$ perpendicular to the edge decreases, and the final result is a normal frazil ice transport that changes little from case to case.

Experiment 3: Varying the wind stress direction. Rotating $\boldsymbol{\tau}$ to be offshore has minimal impact on the polynya shape for the reason already noted in experiment 2. However, as the wind changes from north-northeasterly to northwesterly (Figs. 7a to 7b), the offshore component of the frazil ice drift increases leading to a decrease in both the residence time (from 4 days to about 2.5 days) and maximum thickness (from 0.2 to 0.1 m) of frazil ice. As $\boldsymbol{\tau}$ becomes aligned alongshore (Fig. 7a) a point is reached were no closed polynya is possible. The solution breaks down when no frazil ice trajectory emanating from the coast can reach the polynya ice edge at a given location, a situation shown to be possible in section 3b. South of a point close to the entrance of Ingolfs Fjord (where the polynya does not close in Fig. 7a) the frazil ice trajectories are directed from the domain interior toward the coast. Although there is nothing unphysical in this situation, it is impossible to achieve an ice flux balance. Including a coupling between the wind stress and the oceanic currents could restore, in many cases, a closed solution.

Experiment 4: Varying the magnitude and direction

TABLE 4. Area of the polynya A in each sensitivity experiments

Experiment	Description	A (in km^2)	Change in A (%)	Figure
1	Standard run	4170	0	5
2	Varying the wind stress magnitude			
a		4181	0	6a
b		4170	0	6b
c		4151	0	6c
d		4186	0	6d
3	Varying the wind stress direction			
a		3666	−12	7a
b		4144	−1	7b
c		3951	−5	7c
d		3941	−5	7d
4	Varying the magnitude and direction of the consolidated ice flux			
a		6250	+50	8a
b		1924	−54	8b
c		4811	+54	8c
d		3409	−18	8d
5	Varying the frazil ice production			
a		2478	−41	9a
b		3390	−19	9b
c		5548	+33	9c
d		8159	+96	9d
6	Varying the frazil ice production given by (25)			
a		4837	+16	10a
b		3241	−22	10b
c		—	—	—
7	Varying the ice–ocean drag coefficient	$4126 \leq A \leq 4188$	≤1	—
8	Influence of land fast ice	4396*	5	11
9	Varying the ocean circulation			
a		$4133 \leq A \leq 4231$	≤1	—
b		4206	1	—
c		4143	1	12
11	Consolidated thin ice flux depending on wind and currents			
a		2297	−45	14a
b		6886	+65	14b

* Excluding the area of Ingolfs Fjord.

of the consolidated ice flux. As the magnitude of the consolidated ice flux is increased, while keeping the west-to-east shear constant, the flow of frazil ice across the polynya ice edge must increase so that the ice mass balance is maintained. As illustrated in Fig. 8a, this is achieved by widening the polynya and, hence, enlarging the residence time (~6 days) and increasing the maximum depth (~0.25 m) of frazil ice in the polynya. The opposite response is observed when the consolidated ice flux is decreased (Fig. 8b). As the consolidated ice flux rotates to become more offshore (Fig. 8c) the polynya widens because, again, a larger frazil ice outflow through the polynya ice edge is required to balance the increased consolidated ice flux. Continued rotation of the consolidated ice flux toward a southeasterly direction leads to a situation where no closed polynya is possible. The polynya width decreases as the consolidated ice flux becomes aligned alongshore (Fig. 8d).

Experiments 5 and 6: Varying frazil ice production. As F increases (decreases), the polynya width increases (decreases) in such a way that the total ice production within the polynya (AF) changes remarkably little from one case to another (Fig. 9). Maximum frazil ice depths at the polynya ice edge are fairly similar in all four experiments (of the order of 0.15–0.20 m), whereas residence times in the wider region of the polynya vary from ~2 days in experiment 5a to ~10 days in experiment 5d.

One can argue that for fixed atmospheric conditions the frazil ice production F must depend on the frazil ice depth and concentration, the latter variable not being considered in this simple model. As D increases along the frazil ice trajectories, the upper ocean becomes increasingly thermally insulated from the atmosphere leading to a decrease in F. On this basis we expect larger polynyas will occur if F is allowed to vary with D. To investigate this idea using the steady-state polynya model, the ice production rate is allowed to vary with D according to

$$F(D) = \frac{k_{ai}k_i}{(k_{ai}D + k_i)L_i}(T_f - T_a), \qquad (25)$$

where $k_{ai} = 7$ W m^{-2} K^{-1} is an air–ice exchange co-

efficient, $k_i = 2.0334$ J m^{-1} K^{-1} is the heat conductivity of ice, $L_i = 300.33 \times 10^6$ J m^{-3} is the volumetric latent heat of fusion of ice, $T_f \equiv -1.8$ K is the freezing point of seawater, and T_a is the prescribed surface air temperature. To derive (25), the air–ice heat flux Q_{ai} is balanced by the vertical heat conduction Q_i through the frazil ice in the manner discussed by Willmott and Mysak (1989). We parameterize $Q_{ai} = k_{ai}(T_a - T_s)$ where T_s is the surface temperature of the frazil ice. Although this is a crude parameterization for Q_{ai}, which in reality depends not only on air and surface temperatures but also on factors such as surface wind speed (via the sensible and latent heat fluxes), it is justifiable because $\boldsymbol{\tau}$ is constant. The value of k_{ai} is taken from Willmott and Mysak (1989). Within the frazil ice a linear temperature profile is adopted, in which case $Q_i = k_i(T_s - T_f)/D$. By setting $T_a = -22$°C we find that at the coast, where $D = 0$, $F(0) = 0.04$ m day^{-1}, which is the uniform value used for the frazil ice production in the standard run. Using this value of T_a in (25) leads to a slight widening of the polynya (Fig. 10a) compared with Fig. 5. Maximum frazil ice depths at the polynya ice edge are similar to those in the control run, while the corresponding residence times are ~4 days (half a day larger than in the control case). Upon reducing the air temperature to $T_a = -32$°C we find that $F(0) = 0.06$ m day^{-1} and we obtain an overall increase in frazil ice production compared to the control experiment and a corresponding decrease (Fig. 10b) in the polynya width compared with Fig. 5. Conversely, if $T_a = -12$°C we obtain $F(0) = 0.02$ m day^{-1} and the polynya is too wide to close (not plotted).

Experiment 7: Varying the ice–ocean drag coefficient. For $0.0045 \leq c_{wi} \leq 0.0065$ the polynya shape varies only slightly and therefore no solutions are shown. Since there is uncertainty about the size of c_{wi} it is reassuring that the polynya shape is insensitive to this parameter over a realistic range of values.

Experiment 8: Influence of land fast ice. Figure 11 shows the polynya solution when land fast ice in the inlets and embayments is removed. Comparing Figs. 5 and 11 we see that trajectories within the ice-free bays produce a significant perturbation in the shape of the polynya ice edge.

Experiment 9: Varying the ocean circulation. Solutions calculated for $-10° \leq \lambda \leq 10°$ reveal only minor changes in the polynya shape (not shown) because near the coast the ocean circulation is insensitive to this parameter and because the frazil ice motion is in this experiment basically wind driven. Similarly, decreasing a_2/b_2 from 2 in the standard run to 1.5 leads to a minor change in the polynya shape, and therefore the solution is not plotted. When the oceanic currents are set to 0 (Fig. 12), the frazil ice trajectories are almost perfectly aligned with the wind stress (the Coriolis term is insignificant in this case). There is little change in the area of the polynya compared with the control run, but its shape is significantly modified, reproducing in almost every detail the geometry of the coastline.

Experiment 10: Varying the starting point. Changes in the effective geometry of the coast due to the advance and retreat of fast ice, for example, or in the pack ice motion can lead to variations in the location of the point of intersection between the polynya ice edge and the coastline. Figure 13 shows polynya solutions for different starting points along the southern coast of Nordostrundingen. All contours ''asymptote'' to a common polynya ice edge southwestward of the starting point. In the case when the polynya starts close to the eastern tip of Cape Nordostrundingen, the coastline extent is greater than the alongshore adjustment length scale (14). For the wind stress, oceanic currents, and consolidated thin ice transport used here, polynyas starting at different coastal points in the vicinity of Ob Bank will reach their maximum width (~30 km) some 60 km to the southwest of the starting point, ~60 km.

Experiment 11: Consolidated thin ice flux depending on wind and currents. In the previous experiments, the consolidated thin ice transport is prescribed and it is spatially constant. This is certainly undesirable, and a more complete polynya model should include $\mathbf{T}$ as a prognostic variable depending on the rate of accumulation of frazil ice at the polynya ice edge, the vertical growth of consolidated thin ice, and the consolidated thin ice motion in response to winds and ocean currents. To illustrate the effects of a spatially varying consolidated ice flux on the shape and area of a polynya we have conducted two sensitivity experiments in which the consolidated ice thickness H is assumed to be 0.2 m everywhere, and the consolidated ice velocity $\mathbf{U}$ is calculated as a function of H, $\boldsymbol{\tau}$, and $\mathbf{u}$. In experiment 11a, $\mathbf{U}$ is calculated in terms of the surface wind stress and ocean currents following an empirical relationship proposed by Thorndike and Colony (1982) for the sea ice motion in the central Arctic:

$$\mathbf{U} = A_{TC}(\cos(\theta_{TC})\mathbf{G} - \sin(\theta_{TC})\mathbf{k} \times \mathbf{G}) + \mathbf{u}, \quad (26)$$

where $A_{TC} = 0.008$, $\theta_{TC} = 5°$, $\mathbf{k}$ is an upward unit vector, and $\mathbf{G}$ is the geostrophic wind, related to the surface wind stress via

$$\boldsymbol{\tau} = c_a|\mathbf{G}|(\cos(\theta_G)\mathbf{G} - \sin(\theta_G)\mathbf{k} \times \mathbf{G}), \quad (27)$$

where $c_a = 10^{-3}$ N m^{-4} s^2 and $\theta_G = 28°$ (Overland and Colony 1994). Thus, a geostrophic wind of 10 m s^{-1} leads to a surface wind stress of 0.1 N m^{-2}. In experiment 11b, $\mathbf{U}$ is assumed to obey the free-drift momentum balance (6).

The magnitude of $\mathbf{T}$ obtained by applying the formulation of Thorndike and Colony (1982) tends to be larger than the control value (0.02 m^2 s^{-1}) in the eastern half of the polynya ice edge (Fig. 14a). However, the consolidated thin ice moves to the south-southwest (to the right of the wind), and the ice transport across the polynya ice edge becomes significantly smaller than in experiment 1. In the western half of the polynya ice

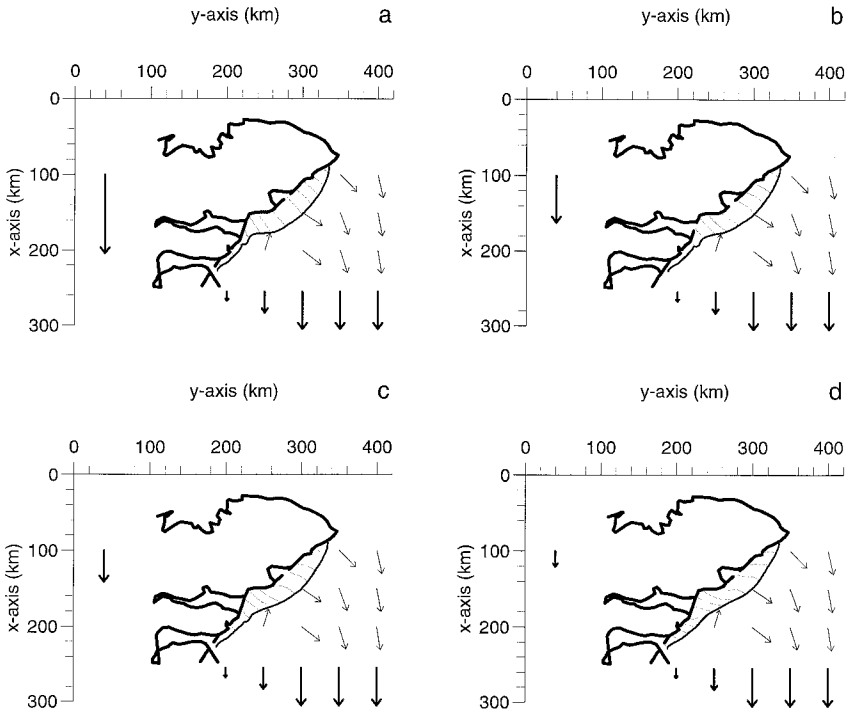

FIG. 6. NEW polynya solutions with varying wind stress magnitude (experiment 2): $|\tau|$ = 0.125 N m^{-2} (a), 0.075 N m^{-2} (b), 0.050 N m^{-2} (c) and 0.025 N m^{-2} (d).

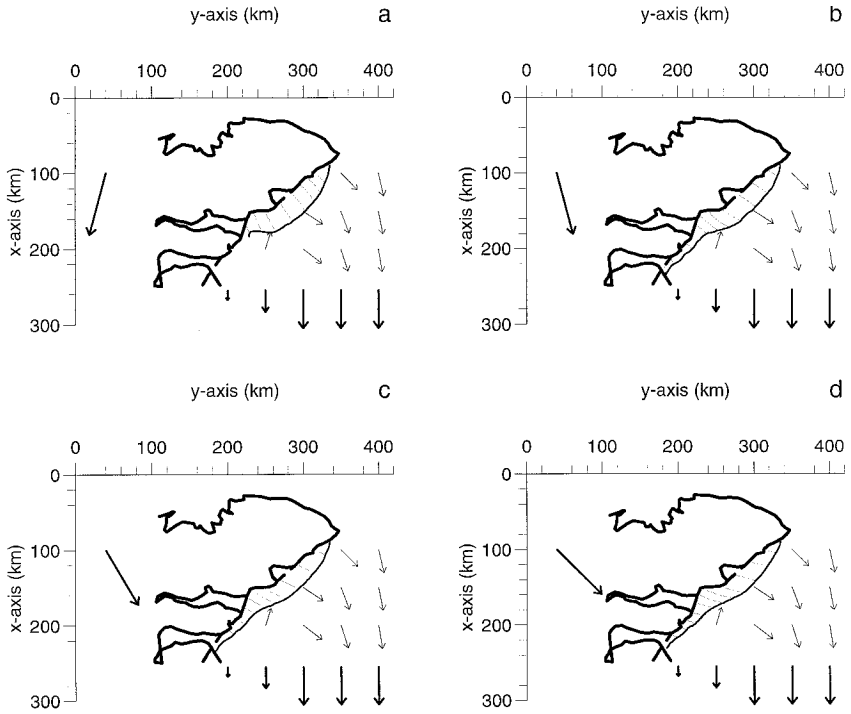

FIG. 7. NEW polynya solutions with varying wind stress direction (experiment 3). θ_a = +15° (a), −15° (b), −30° (c), and −45° (d).

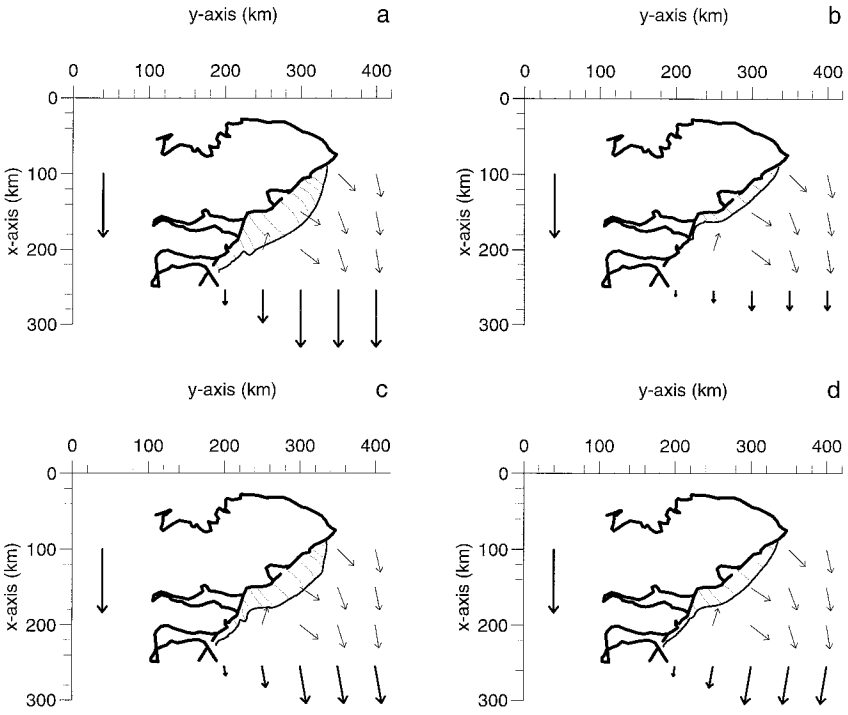

FIG. 8. NEW polynya solutions with varying magnitude or direction of the consolidated ice flux (experiment 4): $|H\mathbf{U}| = 0.03$ m^2 s^{-1} (a), and 0.01 m^2 s^{-1} (b); $\theta_{ci} = -10°$ (c), and $+10°$ (d).

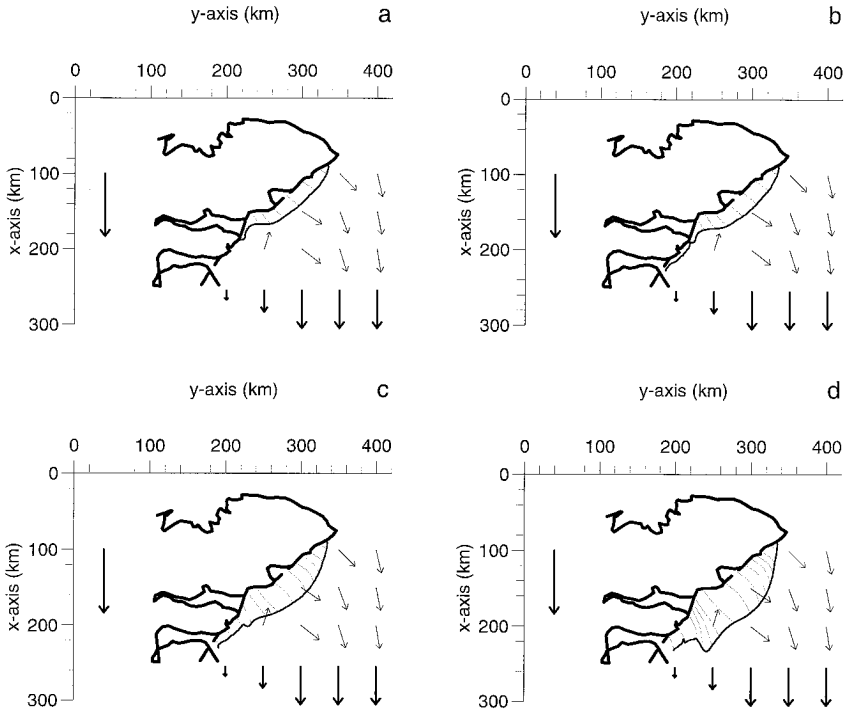

FIG. 9. NEW polynya solution with varying frazil ice production (experiment 5): $F = 0.06$ m day^{-1} (a), 0.05 m day^{-1} (b), 0.03 m day^{-1} (c), and 0.02 m day^{-1} (d).

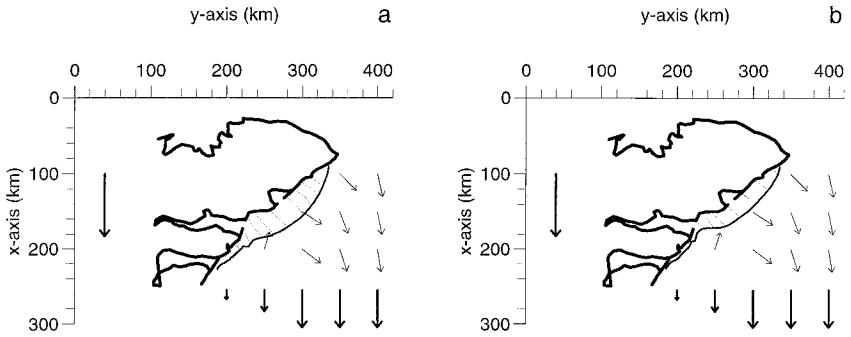

FIG. 10. NEW polynya solutions with frazil ice production varying with frazil ice depth according to (25) (experiment 6): $T_a = -22°C$ (a) and $-32°C$ (b).

edge, $|\mathbf{T}|$ is smaller than in experiment 1 because winds and ocean currents travel in nearly opposite directions. As a result, the steady-state polynya shrinks by about 50% with respect to the control case. In contrast, when $\mathbf{T}$ is calculated using the free-drift momentum balance, the size of the polynya increases considerably (Fig. 14b). In the eastern part of the polynya the consolidated thin ice flux almost doubles that in experiment 1, and it tends to be aligned with the ocean currents. Consequently, the polynya ice edge advances away from the coast and the polynya reaches a maximum width of 60 km. Figures 14a and 14b show the resultant steady-state polynya in experiments 11a and 11b, respectively.

5. Summary and conclusions

A model is developed for determining the size and shape of a steady-state latent heat coastal polynya given the frazil ice production rate (F), wind stress ($\boldsymbol{\tau}$), surface

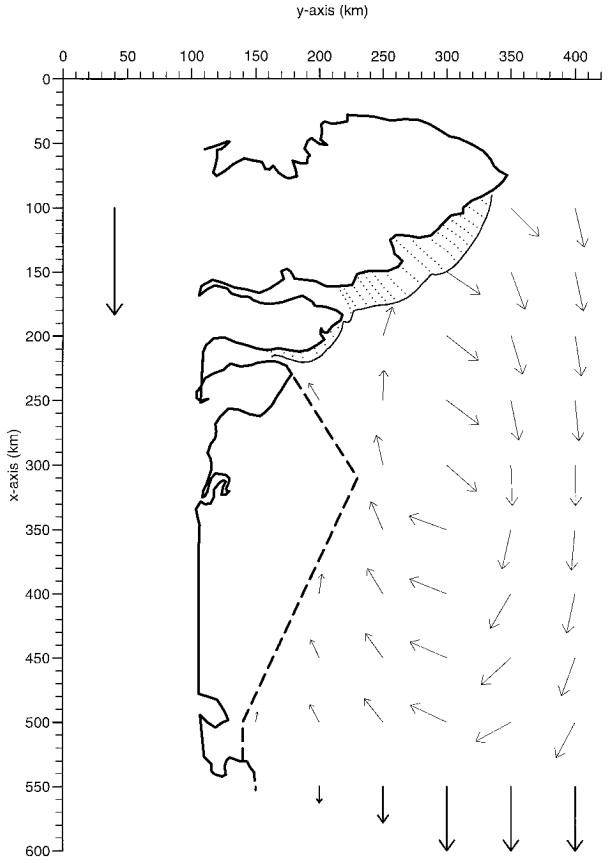

FIG. 11. NEW polynya solution when the three northernmost land fast barriers have been removed (experiment 8). The Norske Ø ice barrier has been retained.

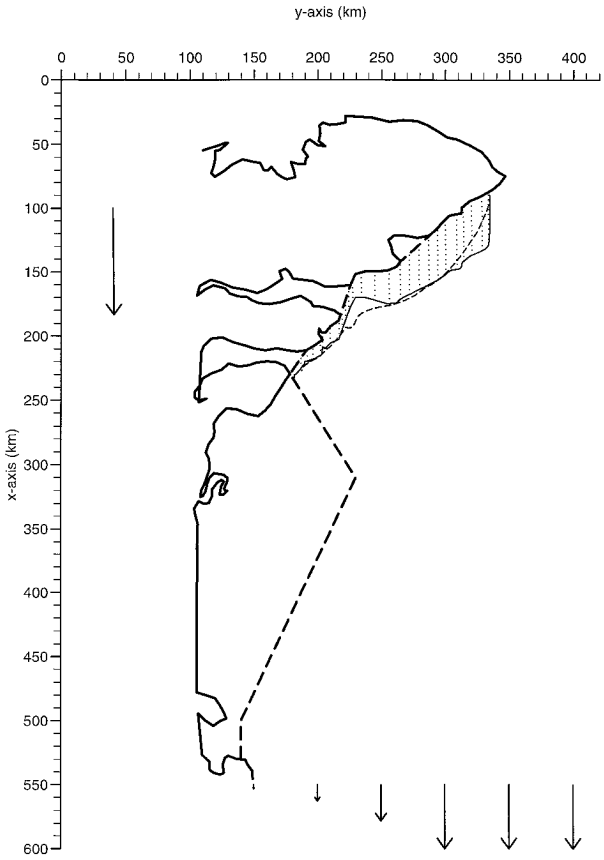

FIG. 12. NEW polynya solution for a stagnant ocean (experiment 9c).

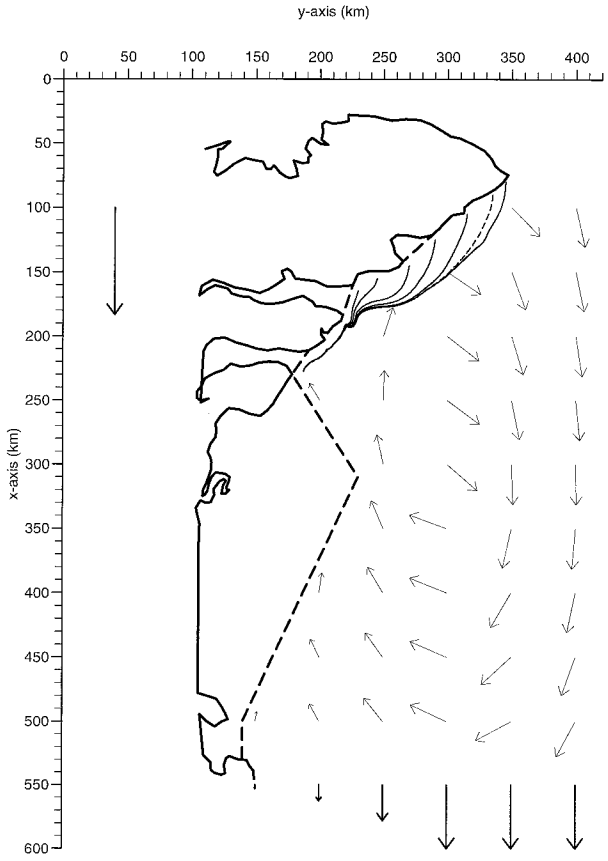

FIG. 13. NEW polynya solutions for a suite of different starting points. The dashed line corresponds to the solution of the control experiment.

ocean circulation (**u**), offshore consolidated ice transport (**T**), the coastline shape, and a point of intersection of the polynya with the coast. The study extends the steady-state polynya model of DWS by allowing the frazil ice trajectories to be determined via the free-drift ice momentum balance, rather than being prescribed.

For a straight coastline it is shown that the polynya asymptotes to a uniform width provided that **u**, $\boldsymbol{\tau}$, and **T** are uniform in the alongshore direction. The polynya width is determined by the offshore component of **T** balancing the frazil ice flux into the polynya ice edge (Pease 1987). The latter flux is given by the integrated frazil ice production rate across the polynya per unit length in the alongshore direction. An expression is also derived for the alongshore adjustment length scale ($L^{(c)}$), which reduces to that in DWS when the frazil ice trajectories are a family of parallel straight lines. In this study $L^{(c)}$ depends not only upon the coastline variations in the alongshore direction (see DWS) but also upon the alongshore variations of $\boldsymbol{\tau}$, **u**, and **T**.

Closed polynya solutions do not always exist in a coastal region. Furthermore, if a point exists on the polynya ice edge where the frazil and consolidated ice fluxes are parallel, the polynya ice edge is not smooth (i.e., no well-defined normal to the edge exists) there. It is shown that all polynya solutions will pass through this critical point. These features are highlighted by calculating the polynya (if it exists) in a wedge-shaped domain with a nondivergent irrotational surface ocean velocity field.

Solutions for the winter and early spring wind-driven polynya in the NEW polynya region are studied using this model. It is also shown how to model the variation of the rate of frazil ice production with the frazil ice depth. This is a potentially important process to consider because in regions where the frazil ice depth builds up we would expect F to decrease. In addition, we have investigated the polynya response when the consolidated thin ice flux at the polynya ice edge is determined as a function of the wind stress and ocean currents. Not surprisingly, the polynya is found to be very sensitive to variations of this flux along the polynya edge. The fact that the two different parameterizations of the consolidated thin ice motion studied here yield very different polynya shapes points to the necessity of using realistic formulations for the consolidated thin ice momentum balance (possibly including internal ice stresses).

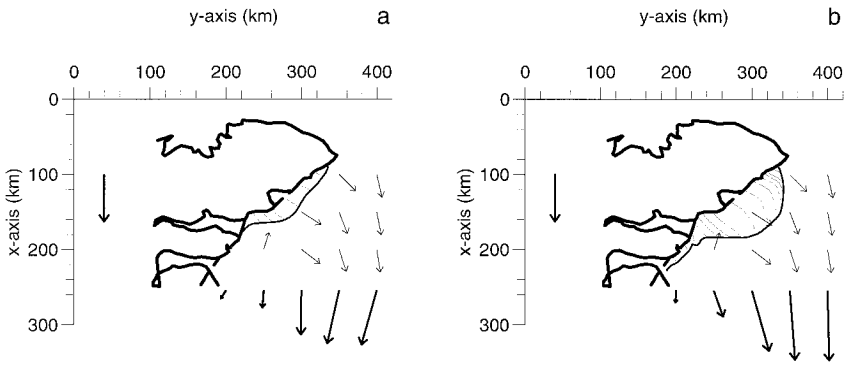

FIG. 14. NEW polynya solutions with consolidated thin ice motion depending on winds and ocean currents (experiment 11): Thorndike and Colony formulation (a) and free-drift balance formulation (b). The vectors representing consolidated thin ice transport have been computed along the line $x = 150$ km.

We stress once more that a fundamental shortcoming of the present study is that the forcing fields of the polynya model (wind stress, ocean currents, frazil ice production, and consolidated ice transport) are decoupled. Obviously, the physical behavior of the polynya is bound to be affected by these couplings, and therefore our senstivity results must be interpreted in the light of this limitation.

A worthwhile extension of this model would be to couple the wind stress field and the ocean circulation in a manner similar to the DWM study of the NOW polynya. Following the DWM approach for modeling the coastal circulation will also allow the oceanic sensible heat flux to be incorporated into the model. For the NOW polynya it is likely that wind-driven upwelling along the West Greenland coast will lead to a significant oceanic sensible heat flux in late spring (DWM).

When an oceanic sensible heat flux associated with coastal upwelling is incorporated into a polynya model this introduces a slow (one to two weeks) adjustment timescale over which the polynya will reach a steady state. This suggests that an unsteady polynya model is worth developing, in a manner similar to that described by Ou (1988).

Between now and the end of the century it is likely that a Canadian-led international program will study the NOW polynya.[1] With the unprecedented high quality data that will become available from the International NOW Study, it is timely to have a range of polynya models that can address how a polynya is formed and maintained. To answer this question for the NOW, the relative contribution of latent and sensible heat processes in maintaining the polynya must be determined. With this in mind the authors are making this model available to the research community and a FORTRAN code will be supplied by the authors upon request.

Acknowledgments. We thank Dr. Mark Johnson for providing us with the digital coastline of the NEW region. We thank Dr. David M. Holland for providing us with a series of charts of sea ice concentration in the Nordic Seas prepared by the Norske Meteorologiske Institutt (1991). We are also grateful to the two anonymous reviewers for suggestions that helped to improve the final version of this paper. M.S.D. gratefully acknowledges support from a U.K. Natural Environment Research Council Advanced Fellowship (GT5/F/92/AAPS/2) while this research was carried out. M.A.M.M. gratefully acknowledges support for a research grant awarded to A.J.W. and M.S.D. via the 4th Round of the Antarctic Special Topic awards administered by the British Antarctic Survey.

[1]Recently it was announced that the NOW project will be funded.

APPENDIX A

Determination of $\mathbf{u}_i$ from the Free-Drift Ice Momentum Balance

In terms of $\mathbf{u}_r = \mathbf{u}_i - \mathbf{u}$, (6) becomes

$$-fDv_r + s_x + c_{wi}u_r(u_r^2 + v_r^2)^{1/2} = 0 \quad \text{(A1a)}$$

$$fDu_r + s_y + c_{wi}v_r(u_r^2 + v_r^2)^{1/2} = 0, \quad \text{(A1b)}$$

where $s_x = -fvD - \tau^x/\rho_i$, $s_y = fuD - \tau^y/\rho_i$, and $\boldsymbol{\tau} \equiv \boldsymbol{\tau}_{ai} = (\tau^x, \tau^y)$. Forming (A1a) v_r − (A1b) u_r and (A1a) u_r, + (A1b) v_r, respectively, yields

$$fDR^2 + \mathbf{k}\cdot(\mathbf{u}_r \times \mathbf{s}) = 0 \quad \text{(A2a)}$$

$$c_{wi}R^3 + \mathbf{u}_r\cdot\mathbf{s} = 0, \quad \text{(A2b)}$$

where $R^2 = u_r^2 + v_r^2$ and $\mathbf{s} = (s_x, s_y)$. In terms of the angle Θ between $\mathbf{s}$ and $\mathbf{u}_r$, (A2) becomes

$$-fDR + |\mathbf{s}|\sin\Theta = 0 \quad \text{(A3a)}$$

$$c_{wi}R^2 + |\mathbf{s}|\cos\Theta = 0. \quad \text{(A3b)}$$

From (A3)

$$\cos\Theta = -\frac{c_{wi}R^2}{|\mathbf{s}|} < 0, \qquad \sin\Theta = \frac{fDR}{|\mathbf{s}|} > 0, \quad \text{(A4)}$$

and

$$\tan\Theta = -\frac{fD}{Rc_{wi}}. \quad \text{(A5)}$$

Clearly, (A4) implies that Θ lies in the second quadrant ($\pi/2 \le \Theta \le \pi$). Using (A4) in the identity $\cos^2\Theta + \sin^2\Theta = 1$ and solving for R^2, we obtain

$$R^2 = \frac{-f^2D^2 + [f^4D^4 + 4|\mathbf{s}|^2c_{wi}^2]^{1/2}}{2c_{wi}^2}. \quad \text{(A6)}$$

Let γ denote the angle between $\mathbf{s}$ and the positive x axis, where

$$\gamma = \arctan\frac{s_y}{s_x}. \quad \text{(A7)}$$

Then

$$u_r = |\mathbf{u}_r|\cos(\Theta + \gamma) = R\cos(\Theta + \gamma) \quad \text{(A8a)}$$

$$v_r = |\mathbf{u}_r|\sin(\Theta + \gamma) = R\sin(\Theta + \gamma), \quad \text{(A8b)}$$

and finally

$$\mathbf{u}_i = \mathbf{u} + \mathbf{u}_r \quad \text{(A9)}$$

provides an expression for $\mathbf{u}_i$ in terms of $\mathbf{u}$, D, and $\boldsymbol{\tau}$ via (A5), (A6), (A7), and (A8).

APPENDIX B

Asymptotic Polynya Width in a Wedge-Shaped Domain

In Figs. 4a and 4c the polynya solutions for the wedge-shaped domain case are observed to asymptote

to a uniform width far from the corner, despite that the alongshore ocean velocity is nonuniform. To understand this behavior we shall first determine an expression for C when $f = 0$. Since $\mathbf{u}_i$ is nondivergent [from (10)] in the absence of rotation, (5b) can be integrated to give $D = Ft$, assuming that on the coastal boundary $D = 0$ when $t = 0$. It is then straightforward to solve (16) for D, and if the initial point of the trajectory is on R_1, then

$$D = \frac{F}{C(1 - p^2)} \times \ln\left(1 + C(1 - p^2)(\rho_i c_{wi}|\boldsymbol{\tau}|)^{1/2}\frac{y - px}{\tau^y - p\tau^x}\right), \quad \text{(B1a)}$$

while if the initial point of the trajectory is on R_2, then

$$D = -\frac{F}{C(1 - p^2)} \times \ln\left(1 - C(1 - p^2)(\rho_i c_{wi}|\boldsymbol{\tau}|)^{1/2}\frac{x - py}{\tau^x - p\tau^y}\right). \quad \text{(B1b)}$$

Clearly, at any point P, D depends only upon the distance from P to the boundary from which the trajectory started. This distance is $(y - px)/(1 + p^2)^{1/2}$ from P to R_1 and $(x - py)/(1 + p^2)^{1/2}$ from P to R_2. It follows that the frazil ice flux through any straight line parallel to either R_1 or R_2 is uniform.

An explicit expression for the frazil ice transport (Du_i, Dv_i) can now be obtained using (10) and (B1), which allows the polynya ice edge slope to be determined from (3). Suppose $V - pU \geq 0$ and $U - pV \geq 0$, which ensure that on R_1 and R_2 the normal component of the consolidated ice transport is directed into the ocean domain. Let $L_1^{(p)}$ denote the asymptotic uniform polynya width far from the corner measured from R_1. Using (3) it can be shown that $L_1^{(p)}$ satisfies the transcendental equation

$$\left(1 + \frac{(1 + p^2)^{1/2}L_1^{(p)}}{T_1}\right)\ln\left(1 + \frac{(1 + p^2)^{1/2}L_1^{(p)}}{T_1}\right) = \frac{H(V - pU)}{FT_1}, \quad \text{(B2a)}$$

where

$$T_1 = (\tau^y - p\tau^x)/(C(1 - p^2)(\rho_i c_{wi}|\boldsymbol{\tau}|)^{1/2}). \quad \text{(B2b)}$$

Similarly, the asymptotic polynya width $L_2^{(p)}$ far from the corner measured from R_2 satisfies the equation

$$-\left(1 + \frac{(1 + p^2)^{1/2}L_2^{(p)}}{T_2}\right)\ln\left(1 - \frac{(1 + p^2)^{1/2}L_2^{(p)}}{T_2}\right) = \frac{H(U - pV)}{FT_2}, \quad \text{(B3a)}$$

where

$$T_2 = (\tau^x - p\tau^y)/(C(1 - p^2)(\rho_i c_{wi}|\boldsymbol{\tau}|)^{1/2}). \quad \text{(B3b)}$$

In the limit $p \to -1$, corresponding to the case when the coastline becomes straight, (B2) and (B3) reduce to the solution $L_1^{(p)} = L_2^{(p)} = H(U + V)/(\sqrt{2}F)$. In general, $L_1^{(p)}$ and $L_2^{(p)}$ depend on $\mathbf{u}$ and $\boldsymbol{\tau}$ as well as $\mathbf{U}$ and F. However, if the magnitude of $\tau^y - p\tau^x$, the offshore component of wind stress to R_1, is sufficiently large or the magnitude of the ocean velocity field is small in the sense that $C \to 0$, then $L_1^{(p)} \to H(V - pU)/[(1 + p^2)^{1/2}F]$. A similar result holds for $L_2^{(p)}$. Conversely, if the wind stress tends to be parallel to the coast or the oceanic currents are very strong, the asymptotic polynya width shrinks.

It is also possible to derive expressions for the alongshore adjustment length scales appropriate to R_1 and R_2. Unfortunately, due to their complexity it is difficult to learn a great deal from them, except to say that their asymptotic limit far from the corner along R_1 and R_2 is infinite, which says that the sensitivity of the polynya ice edge to alongshore variations in the coastline or in the forcing fields will be insignificant in this limit.

Figures 4a and 4b show that with rotation an asymptotic uniform polynya width far from the corner is a robust feature. This a somewhat surprising result because sufficiently far from the origin, the Coriolis term will not remain small, since $|\mathbf{u}|$ increases without bound and hence so will $|\mathbf{u}_i|$. In a rotating environment, the asymptotic balance between the frazil and the consolidated ice fluxes is achieved in the following way. Let us assume for the sake of the argument that $p = 0$ (quarter-plane domain). If an asymptotic polynya width is reached along, say, the x axis, then the asymptotic frazil ice flux through the polynya ice edge is given by

$$\lim_{x\to\infty} Dv_i|_{y=L_1^{(p)}} = HV > 0. \quad \text{(B4)}$$

On $y = L_1^{(p)}$, far from the corner, the ice momentum equations (6) become

$$-fHV - \frac{\tau^x}{\rho_i} + c_{wi}u_r(u_r^2 + v_r^2)^{1/2} = 0 \quad \text{(B5a)}$$

$$fDu_i - \frac{\tau^y}{\rho_i} + c_{wi}v_r(u_r^2 + v_r^2)^{1/2} = 0, \quad \text{(B5b)}$$

upon using (B4), where $\mathbf{u}_r = \mathbf{u}_i - \mathbf{u}$. Since the first and second terms of (B5a) are bounded, $c_{wi}u_r(u_r^2 + v_r^2)^{1/2}$ must also be bounded on $y = L_1^{(p)}$ as $x \to \infty$, which implies that u_r is bounded as $x \to \infty$. Since $u = -Cx$, we deduce that $u_i = O(x)$ as $x \to \infty$.

If we now suppose that v_i is bounded as $x \to \infty$ on $y = L_1^{(p)}$, then the second and third terms of (B5b) are bounded (recall that $v = CL_1^{(p)}$ on the polynya ice edge) and hence $|Du_i| < \infty$ as $x \to \infty$ on $y = L_1^{(p)}$, which contradicts (B4). We therefore deduce that v_i is unbounded as $x \to \infty$ on $y = L_1^{(p)}$, and hence (B4) requires that $D \to 0$ as $x \to \infty$ on the polynya ice edge.

Using (B5) it is straightforward to establish the asymptotic behavior of u_i as $x \to \infty$ on $y = L_1^{(p)}$. We find that

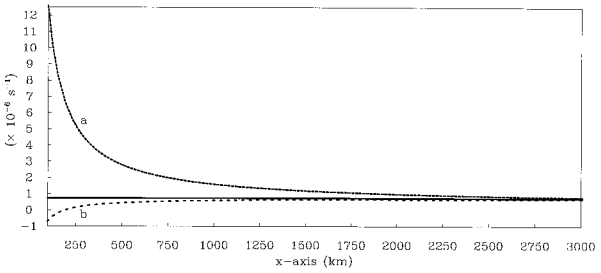

FIG. B1. Plot of $c_{wi}\,(HV)^2(fD^3x)^{-1}$(a) and $-x^{-1}u_i$ (b) on the polynya ice edge in Fig. 4c for a polynya starting at the origin. The asymptote for curves (a) and (b) corresponds to the constant value $C = 7.4 \times 10^{-7}$.

$$D \to 0, \qquad v_i \to \frac{HV}{D}, \qquad u_i \to -\frac{c_{wi}}{f}\frac{(HV)^2}{D^3} = O(x)$$

$$\text{as } x \to \infty \text{ on } y = L_1^{(p)}. \tag{B6}$$

The behavior of D, u_i, and v_i in (B6) contrasts markedly with the nonrotating case in which the asymptotic balance at the polynya ice edge, far from the corner, is achieved with uniform values of D and v_i. With rotation, as the alongshore component of the frazil ice velocity u_i increases with x, the offshore component of the Coriolis force increases, leading to a concomitant increase in v_i. Further, as $x \to \infty$ the length of the frazil ice trajectories increases without bound and they become more aligned with the x axis because from (B6) it is clear that $v_i/u_i \to 0$ as $x \to \infty$. The transit time along the trajectories from the coast (x axis) to the polynya ice edge must also decrease as $x \to \infty$ thereby leading to $D \to 0$ as $x \to \infty$ on $y = L_1^{(p)}$. From (B6) we see that the alongshore frazil ice transport $Du_i \to -c_{wi}\,(HV)^2/(fD^2) = O(x^{2/3})$ as $x \to \infty$.

To confirm the asymptotic behavior (B6), Fig. B1 shows a plot of $c_{wi}(HV)^2(fD^3x)^{-1}$ and $x^{-1}u_i$ as functions of x along the polynya ice edge shown in Fig. 4c. As $x \to \infty$, $c_{wi}(HV)^2(fD^3x)^{-1}$ and $x^{-1}u_i$ both asymptote to the constant value C.

Although it does not appear to be easy to derive an analytical expression for the asymptotic polynya width for this problem with rotation, numerical solutions reveal that the width is bounded above by the nonrotating value. We would expect this upper bound to hold because with rotation the offshore component of frazil ice transport is larger than in the nonrotating case.

REFERENCES

Blumberg, A. F., and G. L. Mellor, 1987: A description of a three-dimensional coastal ocean circulation model. *Three-Dimensional Coastal Ocean Models, Coastal and Stuarine Science,* N. S. Heaps, Ed., Vol. 4, Amer. Geophys. Union, 1–16.

Budéus, G., and W. Schneider, 1995: On the hydrography of the Northeast Water Polynya. *J. Geophys. Res.,* **100,** 4287–4300.

Darby, M. S., and A. J. Willmott, 1993: A simple time-dependent coupled ice-ocean model with application to the Greenland–Norwegian Sea. *Tellus,* **45,** 221–246.

——, ——, and L. A. Mysak, 1994: A nonlinear steady-state model of the north Water polynya, Baffin Bay. *J. Phys. Oceanogr.,* **24,** 1011–1020.

——, ——, and T. Somerville, 1995: On the influence of coastline orientation on the steady state width of a latent heat polynya. *J. Geophys. Res.,* **100,** 13 625–13 633.

Emery, W. J., C. W. Fowler, J. Hawkins, and R. H. Preller, 1991: Fram Strait satellite image-derived ice motions. *J. Geophys. Res.,* **96,** 4751–4768.

Fichefet, T., and M. A. Morales Maqueda, 1997: Sensitivity of a global sea ice model to the treatment of ice thermodynamics and dynamics. *J. Geophys. Res.,* **102,** 12 609–21 646.

Gordon, A. L., and C. Comiso, 1988: Polynyas in the Southern Ocean. *Sci. Amer.,* **258** (6), 70–77.

Johnson, M., and H. J. Niebauer, 1995: The 1992 summer circulation in the Northeast Water Polynya from acoustic Doppler current profiler measurements. *J. Geophys. Res.,* **100,** 4301–4308.

Lebedev, V. L., 1968: Maximum size of a wind-generated lead during sea freezing. *Oceanology,* **8,** 313–318.

Leibovich, S., 1983: The form and dynamics of Langmuir circulations. *Annu. Rev. Fluid Mech.,* **15,** 391–427.

Martin, S., and P. Kauffman, 1981: A field and laboratory study of wave damping by grease ice. *J. Glaciol.,* **27,** 283–313.

Minnett, P. J., 1995: Measurements of the summer surface heat budget of the Northeast Water Polynya in 1992. *J. Geophys. Res.,* **100,** 4309–4322.

Mysak, L. A., and F. Huang, 1992: A latent- and sensible-heat polynya model for the North Water, northern Baffin Bay. *J. Phys. Oceanogr.,* **22,** 596–608.

Norske Meteorologiske Institutt, 1991: Weekly charts of sea ice concentration in the Greenland, Iceland, and Norwegian Seas, Oslo. [Available from Norske Meteorologiske Institutt, P.O. Box 43, Blindern 0313, Norway.]

Ou, H. W., 1988: A time-dependent model of a coastal polynya. *J. Phys. Oceanogr.,* **18,** 584–590.

Overland, J. E., and R. L. Colony, 1994: Geostrophic drag coefficients for the central Arctic derived from Soviet drifting station data. *Tellus,* **46A,** 75–85.

Pease, C. H., 1987: The size of wind-driven coastal polynyas. *J. Geophys. Res.,* **92,** 7049–7059.

Schneider, W., and G. Budéus, 1995: On the generation of the Northeast Water Polynya. *J. Geophys. Res.,* **100,** 4269–4286.

Smith, S. D., R. D. Muench, and C. H. Pease, 1990: Polynyas and leads: An overview of physical processes and environment. *J. Geophys. Res.,* **95,** 9461–9479.

Thorndike, A. S., and R. Colony, 1982: Sea ice motion in response to geostrophic winds. *J. Geophys. Res.,* **87,** 5845–5852.

Willmott, A. J., and L. A. Mysak, 1989: A simple steady-state coupled ice-ocean model, with application to the Greenland–Norwegian Sea. *J. Phys. Oceanogr.,* **19,** 501–518.